Published in final edited form as:
Nat Cancer. 2020 February ; 1(2): 210–221. doi:10.1038/s43018-019-0022-x.

Immune-awakening revealed by peripheral T cell dynamics after one cycle of immunotherapy

Sara Valpione[1,2], **Elena Galvani**[1], **Joshua Tweedy**[1], **Piyushkumar A. Mundra**[1], **Antonia Banyard**[3], **Philippa Middlehurst**[4], **Jeff Barry**[3], **Sarah Mills**[4], **Zena Salih**[2], **John Weightman**[5], **Avinash Gupta**[2], **Gabriela Gremel**[1,6], **Franziska Baenke**[1,7], **Nathalie Dhomen**[1], **Paul C. Lorigan**[2,*], **Richard Marais**[1,*]

[*]**Corresponding authors:** Prof Paul Lorigan, The Christie NHS Foundation Trust, 550 Wilmslow Road, Manchester M20 4BX, United Kingdom, paul.lorigan@christie.nhs.uk; Prof Richard Marais, Molecular Oncology Group, CRUK Manchester Institute, The University of Manchester, Alderley Park SK10 4TG, United Kingdom, Tel: +44 (0)161 306 6017, richard.marais@cruk.manchester.ac.uk.
[6]current affiliation: Boehringer Ingelheim RCV GmbH & Co KG, Vienna, Austria
[7]current affiliation: German Cancer Consortium (DKTK) German Cancer Research Centre (DKFZ), Heidelberg, Germany and Department of Visceral, Thoracic and Vascular Surgery, University Hospital Carl Gustav Carus, Technical University Dresden, Germany.

Data Availability

Sample metadata file are available from GitLab (https://gitlab.com/cruk-mi/tcell-immune-awakening). The data from all TCR sequencing performed for this study are deposited in ImmunoSEQ® Immune ACCESS repository (https://clients.adaptivebiotech.com/immuneaccess). The RNA-Seq data for patient #12 can be downloaded from EGA (accession code EGAS00001004043). TCR sequencing data for matched pre-treatment and week 3 melanoma biopsy and PBMC samples of locally-advanced melanoma patients[18] re-analyzed here were downloaded from referenced accession EGAS00001003178 EGA study accession dataset EGAD00010001608. TCR sequencing data of matched pre-treatment and week 3 melanoma patient PBMC from AC Huang *et al.*[7] re-analyzed here were kindly made available by the Authors. TCR sequencing data of matched pre-treatment and week 3 PBMC for the cohort of locally-advanced treatment naive melanoma patients from referenced accession Amaria *et al.*[18] re-analyzed here were downloaded from EGAS00001003178 EGA study accession dataset EGAD00010001608, patient clinical history metadata file from EGAD00001004352. PBMC and biopsy CyTOF data from Krieg *et al.*[8] and Greenplate *et al.*[24] re-analyzed here were downloaded from referenced accession https://flowrepository.org/experiments/1124 and http://flowrepository.org/id/FR-FCM-ZZMC, respectively. PBMC REAP-Seq data from Peterson *et al.*[27] re-analyzed here were downloaded from referenced accession https://www.ncbi.nlm.nih.gov/geo/query/acc.cgi?acc=GSE100501. The authors confirm that, for approved reasons (UK Data Protection Act 2018), some access restrictions apply to data containing patient medical records (date of birth). Source data for Fig. 1-7 and Extended Data Fig. 3-6 are provided as Source Data files Fig. 1-7 and Extended Data Fig. 3-6. Additional data that support the findings of this study are available from the corresponding author on reasonable request.

Code Availability

ImmunoSEQ® ANALYZER (Adaptive Biotechnologies, Seattle, WA, USA), FlowJo (v.10, Tree Star Inc., Ashland, OR, USA), Cytobank[55], Trimmomatic (v0.36)[49] and STAR (v2.5.1) aligner[50] are published or commercial codes and softwares. Diversity was calculated using Renyi index (α=1) as per Spreafico *et al.*[52]. Differential marker expression analysis was performed on CyTOF data was performed using the custom workflow described in Nowicka *et al.*[53]. Custom R scripts are available in GitLab (https://gitlab.com/cruk-mi/tcell-immune-awakening).

Conflict of Interest: RM is a consultant for Pfizer and has a drug discovery programme with Basilea Pharmaceutica. PL serves as paid advisor/speaker for Bristol-Myers Squibb, Merck Sharp and Dohme, Roche, Novartis, Amgen, Pierre Fabre, Nektar, Melagenix. PL reports travel support from Bristol-Myers Squibb and Merck Sharp and Dohme, and receives research support from Bristol-Myers Squibb. AG received honoraria and consultancy fees from BMS and Novartis.

Author Contributions

Conception and design: SV and RM
Development of methodology: SV, ND, RM
Acquisition of data (managed patients, provided facilities, provided bioinformatics supervision, performed experiments etc.): SV, EG, PAM, AB, PM, JB, JT, GG, AG, SM, ZS, FB, JW, ND, PCL, and RM
Analysis and interpretation of data (e.g., statistical analysis, biostatistics, computational analysis): SV, ND, RM
Graphics preparation: SV, AB
Writing of the manuscript: SV, ND and RM, with input and final approval of all authors.

Europe PMC Funders Author Manuscripts

[1]Molecular Oncology Group, Cancer Research UK Manchester Institute, The University of Manchester, Alderley Park SK10 4TG, United Kingdom

[2]The Christie NHS Foundation Trust, 550 Wilmslow Road, Manchester M20 4BX, United Kingdom

[3]Advanced Imaging and Flow Cytometry, Cancer Research UK Manchester Institute, The University of Manchester, Alderley Park SK10 4TG, United Kingdom

[4]Manchester Cancer Research Centre Biobank, The Christie NHS Foundation Trust, 550 Wilmslow Road, Manchester M20 4BX, United Kingdom

[5]Molecular Biology Core Facility, Cancer Research UK Manchester Institute, The University of Manchester, Alderley Park SK10 4TG, United Kingdom

Abstract

Our understanding of how checkpoint inhibitors (CPI) affect T cell evolution is incomplete, limiting our ability to achieve full clinical benefit from these drugs. Here we analyzed peripheral T cell populations after one cycle of CPI and identified a dynamic awakening of the immune system revealed by T cell evolution in response to treatment. We sequenced T cell receptors (TCR) in plasma cell-free DNA (cfDNA) and peripheral blood mononuclear cells (PBMC) and performed phenotypic analysis of peripheral T cell subsets from metastatic melanoma patients treated with CPI. We found that early peripheral T cell turnover and TCR repertoire dynamics identified which patients would respond to treatment. Additionally, the expansion of a subset of immune-effector peripheral T cells we call T_{IE} cells correlated with response. These events are prognostic and occur within 3 weeks of starting immunotherapy, raising the potential for monitoring patients responses using minimally invasive liquid biopsies."

Introduction

T cell maturation begins when pro-T cells enter the thymus and attempt to generate a functional T cell receptor (TCR). Cells that fail to do so are eliminated through β-selection, but those that succeed must still pass positive and negative (+/-) selection for HLA binding and absence of reactivity to self-antigen in order to survive (Extended Data Fig. 1a,b). Successful naïve T cells enter the circulation as early thymic emigrants (ETE), and if stimulated by antigen presenting cells in the lymphatic system, they expand and migrate to sites of inflammation to combat harmful agents, a process that resolves through clonal contraction and more T cell death[1] (Extended Data Fig. 1c-e).

Checkpoint inhibitor (CPI) drugs awaken the immune system so that they attack tumors. CPI have revolutionized cancer care and, over the last decade, have contributed to a 4-fold improvement in the survival of metastatic melanoma patients[2]. Despite these remarkable advances, our understanding of T cell evolution under the selective pressure of CPI is still incomplete and that limits our ability to derive full clinical benefit from these drugs. Consequently, most patients with advanced stage melanoma still die of their disease. Sharing features with responses to infectious diseases[3–5], tumor control by the immune system requires coordination between systemic and intra-tumoral immunity[6], and although several studies have investigated intra-tumoral responses to immunotherapy[7–9], few have focused on

how CPIs affect the peripheral immune system, or whether changes in peripheral T cells are associated with patient responses[7,8,10].

We hypothesized that because immune responses to tumors mirror normal defensive responses to pathogens, it would be possible to study patient responses to CPI by monitoring peripheral T cell evolution during treatment. T cell receptors (TCR) are generated by error-prone recombination of the *TCR* locus[11,12], creating the enormous diversity needed for effective immune function. This process is ~80% efficient, so most peripheral T cells carry only productive *TCR* sequences. However, in ~20% of peripheral T cells the first attempts at *TCR* locus rearrangement failed due to acquisition of stop codons or because the protein coding region was out of frame, so these T cells carry both productive and non-productive *TCR* sequences[13]. The complementarity determining region-3 (CDR3) of the TCR in particular is highly variable and the sequences are unique to individual T cell clones, so both the productive and non-productive *TCR* sequences serve as a "fingerprints" for individual T cell clones.

We posited that by sequencing peripheral T cell *CDR3* regions, we could track T cell responses to CPI and, because dying cells release their DNA into the circulation, we could also sequence *CDR3* regions in cell free DNA (cfDNA) in the blood to monitor T cell turnover in patients receiving CPI. We found an increase in productive TCR sequences in plasma cfDNA of patients who responded to CPI, and this correlated with response. These events were accompanied by evolution of the peripheral T cell repertoire in a manner that mimicked changes induced by anti-viral vaccines. The dynamics of T cell turnover revealed by the cfDNA analysis also correlated with expansion of a specific subset of cytotoxic memory effector peripheral T cells we call immune-effector or T_{IE} cells. Importantly, T_{IE} cell expansion after one cycle of CPI anticipated which patients would go on to respond to treatment. Our data reveal an awakening of the immune system that occurs within 3 weeks of initiating CPI and which anticipates clinical response to first-line therapy. These changes are dynamic and quantifiable and can be monitored with minimally invasive liquid biopsies, features that could be used to identify which patients will benefit from CPI early during their treatment, allowing delivery of more precise treatment planning.

Results

Immunotherapy does not alter thymic output

First, we examined the effects of CPI on thymic function. We used fluorescent-activated cell sorting (FACS, Extended Data Fig. 2) to quantify the ETE ($CD3^+/CD45RA^+/CD45RO^-/CCR7^+/CD27^+/CD31^+$ T cells[14]) in peripheral blood mononuclear cells (PBMC) from 50 metastatic melanoma patients (#1-50) receiving first-line anti-PD1 or anti-PD1/anti-CTLA4 treatment (Extended Data Fig. 2i). As expected[15], we observed an age-related decrease in ETE levels in pre-treatment (T0) patient blood (Fig. 1a), but we also found that one cycle of CPI did not affect ETE levels, measured at week 3 (W3)(P=0.274; Fig. 1b). Next, we examined the TCR excision circle (TREC) in the peripheral T cells of 16 of our patients (#1,10-13,22,24-27,30,42,51-54). The TREC, a by-product of *TCR* locus rearrangements, is a non-replicating episome that is diluted when T cells divide[16] (Extended Data Fig. 1a-d). We found that the TREC:genome ratio in T cells was not affected by CPI (P=0.129, Fig. 1c).

CPI induce TCR repertoire divergence in peripheral T cells

The observations above indicate that CPI did not affect thymic output in melanoma patients, so to monitor how CPI affected post-thymic T cell evolution, we analyzed the TCR in peripheral PBMC and melanoma metastases. For patient #12 we obtained a fresh tumor biopsy at T0, and whole blood at T0 and after the first cycle of CPI at W3. Using ImReP[17] we identified 16 unique *CDR3* DNA sequences from the biopsy and found that 6 of these were also present in the PBMC and cfDNA (Fig. 1d, Table 1). Thus, about one third of the sequences in the tumor were also in the periphery, four in pre-treatment PBMC (sequences $CDR3_{DNA1.1}$, $CDR3_{DNA1.2}$, $CDR3_{DNA2.1}$, $CDR3_{DNA3}$), three in the W3 PBMC ($CDR3_{DNA1.1}$, $CDR3_{DNA2.1}$, $CDR3_{DNA2.2}$), and one in the W3 cfDNA ($CDR3_{DNA4}$)(Table 1). Intriguingly, $CDR3_{DNA1.1}$ and $CDR3_{DNA1.2}$ both encoded TCR $CDR3_{prot1}$ (Table 1), and $CDR3_{DNA2.1}$ and $CDR3_{DNA2.2}$ both encoded $CDR3_{prot2}$ (Table 1), suggesting convergence by these TCR on dominant tumor antigens. We also analyzed *CDR3* sequences in 18 paired PBMC and TIL from a published melanoma cohort[18]. As an example, at T0 patient #01 presented 123,981 unique *CDR3* sequences in the bulk PBMC, 21,052 in the TIL and 3,741 shared sequences (Fig. 1e), comparable patterns were seen in the other patients (Supplementary Table 1).

These data established that tumor resident T cell clones were also present in the periphery, so we called these cells tumor-emigrant PBMC (tePBMC). We compared the clonal relatedness[19,20] of the CDR3 regions from the tePBMC to the PBMC-private and TIL-private pools. At T0, the tePBMC and TIL-private TCR pools displayed more clonal relatedness than the PBMC-private CDR3 regions (Fig. 1f), suggesting more TCR convergence in tumor-associated T cells than the bulk PBMC population. At week 3, we did not observe differences in clonal relatedness in the PBMC-private or TIL-private TCR when we compared patients who achieved disease control (DC) at week 12 with those who developed progressive disease (PD) (Extended Data Fig. 3a). Similarly, when we compared clonal relatedness in the PBMC-private TCR at T0 and W3, we did not observe differences between DC or PD patients, whereas in the tePBMC pool, there was a significant reduction in TCR clonal relatedness in patients who achieved PD, but not in patients who had PD (Fig. 1g). This suggests recruitment of T cells with a broader TCR repertoire from the periphery to the tumors of patients who responded, but not to the tumors of patients who did not respond.

CPI induce peripheral T cell turnover

Next, we compared the CDR3 clonal relatedness in PBMC and cfDNA of 28 CPI-treated metastatic melanoma patients (#11-27,#29-39). In T0 blood from patient #27 we observed 14,112 unique *CDR3* sequences in the bulk PBMC, 844 in the cfDNA and 193 shared sequences (Fig. 2a). Comparable patterns were seen in the other 27 patients (Supplementary Table 2). Intriguingly, the number of unique PBMC/cfDNA-shared CDR3 sequences increased after one cycle of CPI (Fig. 2b), so we investigated how CPI affected the immune-recognition landscape in these pools. At T0 the PBMC-private CDR3 clonal relatedness was ~0, but was significantly higher in both the cfDNA-private and PBMC/cfDNA-shared pools (Fig. 2c). Critically, clonal relatedness in the PBMC/cfDNA-shared pool decreased

significantly in patients who achieved DC at week 12, but not in patients with PD (Fig. 2d), suggesting repertoire divergence in the T cells that turnover in the responding patients.

The cfDNA *CDR3* sequences come from T cell turnover in the thymus and periphery and contain both productive and non-productive sequences (Extended Data Fig. 1). We used ImmunoSeq to quantify productive (reading frame intact) and non-productive (out of frame, stop codon) *CDR3* sequences and calculate a Rearrangement Efficiency Score (RES; productive/[productive+non-productive]). In healthy donors (HD) the PBMC RES was ~0.8 as expected[13], but in cfDNA the RES was 0.44 ($P<0.001$; Fig. 2e), presumably from non-productive *TCR* sequences released by T cells failing β-selection in the thymus. The T0 PBMC and cfDNA RES (RES_{T0}) values were similar in HD and patients (Fig. 2e), suggesting that melanoma does not overtly affect the efficiency of T cell rearrangements in the thymus and also that it does not affect bulk T cell turnover in the periphery. We therefore compared the RES in PBMC and cfDNA at T0 and W3 to generate difference scores (Δ_{W3}RES) and measure how CPI affects T cell rearrangement and turnover during the first cycle of immunotherapy. The PBMC Δ_{W3}RES measured changes in *TCR* rearrangement efficiency and was ~0 irrespective of whether the patients responded or not (Fig. 2f). Thus, CPI did not affect *TCR* rearrangement efficiency in the thymus, meaning that the cfDNA Δ_{W3}RES measured the changes in the peripheral T cell turnover alone. Notably, the cfDNA Δ_{W3}RES rose from ~0 in patients with PD to 0.09 ($P=0.037$) in patients who achieved DC at 12 weeks (Fig. 2f). Thus, CPI increased peripheral T cell turnover in responding patients, but not in non-responding patients.

CPI stimulate expansion of specific peripheral T cell subsets

Our data reveals dynamic TCR repertoire reorganization during T cell expansion/contraction in responding patients, so we used high dimensional FACS to characterize peripheral T cell subsets and monitor T cell evolution under CPI (Extended Data Fig. 2). We found that a $CD8^+$ memory effector cytotoxic T cell subset that we called immune-effector T cells (T_{IE}) expanded proportionally to the cfDNA Δ_{W3}RES (Fig. 3a). T_{IE} cells are characterized by the surface phenotype $CD3^+/CD4^-/CD8^+/CD45RA^-/CD45RO^{high}/CD27^-/CCR7^-$ (Extended Data Fig. 1k) and have been shown to be associated with response to infections[21,22].

To study cytotoxic T cell turnover, we sequenced the *TCR* in T0 and W3 purified $CD8^+$ peripheral memory and naive T cells from 3 PD and 3 DC patients (#12,16-19,29). More than other peripheral T cell subsets, the T_{IE} cells had the highest similarity to cfDNA *CDR3* sequences (Fig. 3b) and presented the highest clonality (Fig. 3c). This suggests T_{IE} cells are actively turning over, but with convergence towards dominant clones. Moreover, although it is not yet possible to establish if the T_{IE} cell CDR3 regions recognized neo-epitopes, largely these cells did not express TCR known to recognize public epitopes such as Melan-A or viral proteins (Supplementary Table 3). In patient #12, from whom we obtained a biopsy, we identified identical CDR3 sequences in the tumor and the peripheral T_{IE} cells (Fig. 3d), demonstrating that individual T_{IE} clones coexisted in the tumor and periphery. Moreover, expansion of intratumoral cells with the T_{IE} phenotype is reported to be associated with responses to CPI[23], and we used published CyTOF data[24] to confirm that T_{IE} cells were

resident in melanoma and renal cell carcinoma (immune-responsive tumors), but were negligible in glioblastoma (immune-refractory tumor) and tonsils (Fig. 4a-d).

Next, we analyzed PBMC from 30 CPI-treated metastatic melanoma patients from our cohort (#1-30) and show that the T_{IE} cells expanded at W3 in patients who achieved DC, including late responders, but not patients with PD (P=0.0007; Fig. 5a), irrespective of therapy protocol (P=0.200, Fig. 5b). Notably, despite a W3 T_{IE} expansion of ~20%, the W12 CT scan revealed that patient #20 was progressing (Fig. 5a). Unfortunately, the patient died of complications so a late response could not be measured, but from day 40 we observed a steady decline in this patient's *NRAS*^{Q61R} circulating tumor DNA (ctDNA)[25] (Fig. 5c), revealing that consistent with the observed expansion in T_{IE} cells, the patient achieved a biochemical response (Fig. 5c). An increase of >0.8% in the T_{IE} ratio relative to all CD8^{+} memory T cells at W3 was associated with increased overall survival and segregated DC (including late-responders) from PD patients with sensitivity = 0.94 and specificity = 0.79 (accuracy = 0.87 and area under the curve [AUC] = 0.85) (Fig. 5d). The Hazard Ratio for patients without W3 T_{IE} expansion was 3.7 (95% CI 1.12-11.9, P=0.032) (Fig. 5e). We confirmed these observations in an independent cohort of 20 CPI-treated patients (#31-50, Fig. 5f,g), with sensitivity = 0.82 and specificity = 1 (accuracy = 0.90, AUC = 0.92). By week 9, T_{IE} cells no longer discriminated DC from PD patients (Extended Data Fig. 4a). Accordingly, when we analyzed published CyTOF data[3], we confirmed T_{IE} to be a distinct T cell subset in PBMC of patients with metastatic melanoma (Extended Data Fig. 4b,c), but consistent with our findings, the T_{IE} levels at week 12 did not distinguish DC from PD patients (Extended Data Fig. 4d). Thus, changes at W3 were prognostic for melanoma responses to CPI, but were no longer prognostic by W9 or W12, demonstrating the dynamic nature of these responses and consistent with a previous study showing that the peak of immune activation is at W3[7,10].

We note that the W3 T_{IE} expansion identified patients who achieved DC early during treatment with superior accuracy to the W3 peripheral T lymphocyte invigoration to tumor burden ratio (Ki67/TB), where the accuracy = 0.64 (16/24 patients with Ki67/TB>1.94 had an objective response compared to 3/17 patients with Ki67/TB<1.94)[7]. We note also that the W3 T_{IE} expansion also had greater accuracy than PD-L1 staining in pre-treatment melanoma biopsies where the accuracy in a phase III clinical trial = 0.67 (78/148 patients with PD-L1 positive biopsy had an objective response compared to 89/270 patients with PD-L1 negative biopsy)[26].

Next, we analyzed published single cell RNA expression and protein sequencing (REAP-Seq) data from healthy donors[27] and found that T_{IE} cells have the additional surface phenotype CD69^{+}/PD1$^{low/dim}$/TIGIT^{+}/CD25$^{+/-}$/CD155^{+}/CD40$^{med/high}$/CD154$^{med/high}$/CD357$^{med/high}$ and a distinct transcriptome signature including immune-activation genes (cluster 9 in Extended Data Fig. 5a,b and Supplementary Table 4). Our analysis of this data also showed that T_{IE} cells expanded from healthy donor CD8^{+} naive PBMC following *in vitro* stimulation, and that they expressed genes associated with immune-effector function (Extended Data Fig. 5c-d). Using FACS analysis of 5 patients' PBMC (#1,24,29,42,54) we observed a trend for T_{IE} reinvigoration (increased Ki67^{+} expression) after 1 cycle of CPI (Extended Data Fig. 6a), although the limited sample size could not support robust

Europe PMC Funders Author Manuscripts

conclusions. Note that the W3 T_{IE} expansion was not associated with toxicity, but expansion of a separate T regulatory (T_{reg}) subset characterized by surface phenotype $CD3^+$/$CD4^+$/$CD8^-$/$CD25^+$/$CD127^{-/low}$[28] correlated with toxicity grade (Fig. 6a,b).

CPI induce peripheral T cell repertoire rearrangements

Our findings revealed intriguing parallels between immune responses to infection[21,22] and CPI, and we hypothesized that immune responses to CPI mirror the defense against pathogens. To test this, we compared T cell repertoire rearrangements in people receiving vaccination or CPI. Using published data[29,30], we calculated T cell clonality (measures clone dominance) and diversity (indicates heterogeneity) and note that 1-2 weeks after anti-viral vaccines were administered, healthy donor TCR repertoires presented bifurcated reorganization with either increased clonality or increased diversity (Fig. 7a). We next compared clonality (Δ_{W3}clonality) and diversity (Δ_{W3}diversity) in T0 and W3 PBMC from 17 CPI-treated metastatic melanoma patients (#11-27). In patients who went on to achieve DC at week 12 we observed bifurcated reorganization of the TCR repertoire, with substantially increased clonality or diversity, whereas no such response occurred in patients with PD (Fig. 7b). Using our training cohort, we developed a linear discriminant analysis (LDA) algorithm that at W3 classified patients according to response (assessed at week 12) with an accuracy of 0.9 (specificity=1 and sensitivity=0.8). We validated these findings in an independent cohort of 27 patients with advanced melanoma[7,31], and again found a bifurcated TCR repertoire reorganization in DC, but not PD patients (Fig. 7c). Our LDA accuracy for response prediction was 0.77 in this validation cohort.

Discussion

We examined how the selective pressure of a single cycle of CPI affects peripheral T cell evolution in previously untreated metastatic melanoma patients. We found that CPI induced immune-awakening that was revealed by increased levels of productive *CDR3* sequences released into the blood and dynamic changes in the TCR repertoire. CPI did not affect thymic output but did induce peripheral T cell turnover and this correlated with the expansion of a $CD8^+$ cytotoxic memory effector subset that was $CCR7^-$/$CD27^-$. This subset of lymphocytes is involved in cytotoxic response to infections[32,33] and we have now established that they are also associated with CPI responses. Immune effector cells are the cells of the immune system that support anti-cancer immune surveillance[34], and since our data has identified a specific T cell subset involved in this network, we called them immune-effector T cells, or T_{IE} cells.

It was recently shown that following CPI treatment, the expansion of tumor infiltrating T cell clones did not come from pre-existing TIL[35], but rather from novel clonotypes, most probably in the peripheral compartment. Those observations are consistent with a model that the tumor is an open compartment with active cross-talk with the peripheral immune-system and accordingly, in responding patients we observed a significant early T cell repertoire rearrangement in the fraction of TIL circulating in the blood, and which we call tumor emigrant T cells or tePBMC.

Clonotype modulation by checkpoint blockade has been described previously, largely in the tumor microenvironment[7,36–38], but we determined that the pattern of peripheral turnover and overall repertoire rearrangement of T cells in blood identify the patients with an effective immune-awakening and who will go on to respond to CPI. It has also been shown in animal models that anti-CTLA4 and anti-PD1 drugs induce distinct cellular reactions[39]. That we did not observe significant differences between single-agent and anti-PD1/CTLA4 combined therapy supports that our observations reflect the final effects needed for tumor elimination, and importantly we showed that these changes could be detected in the periphery. Although we could not discriminate if the T cell clones driving these changes were melanoma-specific, or if this reflected a general, off-target immune-activation, our results nonetheless contribute to our understanding of the dynamics of immune-system evolution after one cycle of CPI. That these responses also occur with infection could limit specificity in the CPI setting, necessitating further kinetic analysis and clinical validation, but our results have established that these responses could provide tractable tools for the delivery of precision immunotherapy. Moreover, our hypothesis-generating results contribute to improved understanding of immune system biology and they could have broader implications beyond the oncoimmunology field.

Note that CCR7 and CD27 were downregulated in T_{IE} cells, and that phenotype has been associated with differentiated effector T cell release from lymph nodes to the periphery[40–43]. Also in line with previous observations that *in vitro* stimulation of CD8+ T cells induced downregulation of CD27 and CCR7[44,45], our analysis of previous data showed that T_{IE} cells expanded following *in vitro* stimulation. Our data also showed that the expansion of these cells after one cycle of CPI identified the patients for whom therapy overcame melanoma-induced immune-suppression. Within the scope of this study, we have not analyzed the anti-tumor reactivity of T_{IE} cells, but our data showed that peripheral T_{IE} clones infiltrated melanoma and represent an abundant fraction of tumor infiltrating lymphocytes with high repertoire clonality. The T_{IE} were also in active turn-over. The relatively small size of our sample could limit the generalization of our results, but both T_{IE} and TCR peripheral repertoire reorganization could identify which patients will benefit from CPI with greater accuracy than standard biopsy PD-L1 staining or Ki67/TB. Future research will investigate the anti-tumor cytotoxicity and specificity of these cells, and their potential for clinical development.

In summary, here we identified a peripheral blood early immune-signature characterized by significant rearrangements of the peripheral T cell repertoire and by turnover of specific T cell subsets. Critically, the magnitude of the immune-signature changes after the first cycle of therapy anticipated which patients would go on to respond and were detected in the blood, providing the advantages inherent in minimally invasive liquid biopsies. Although further studies are required to determine the mechanisms underpinning our observations and their specificity for CPI-induced responses, our research provides a strategy to analyze immune cell evolution under the selective pressure of CPI. Our findings advance our knowledge of immune system responses to immunotherapy, and critically they provide a potentially tractable tool to identify which patients will benefit from CPI early during treatment. This could help clinicians to stratify their patients more effectively to thereby improve personalization of therapeutic planning.

Materials and Methods

Patient samples

Blood samples from patients and healthy donors were collected under the Manchester Cancer Research Centre (MCRC) Biobank ethics application #07/H1003/161+5 with written informed consent from the patients at The Christie NHS Foundation Trust. The study was approved by MCRC Biobank Access Committee application 13_RIMA_01. All clinical investigations were conducted according to the principles expressed in the Declaration of Helsinki and good clinical practice guidelines. A total of 54 patients with metastatic melanoma, treated with either pembrolizumab or nivolumab plus ipilimumab as first-line therapy as per standard of care were included in the study. Inclusion criteria: the diagnosis of metastatic melanoma; exclusion criteria: previous systemic oncological treatment in the neoadjuvant, adjuvant or metastatic setting for melanoma or other cancers, concomitant therapy with immunosuppressant drugs at enrolment and synchronous other active malignancies. With the exception of two patients who had rapid, severe unequivocal clinical disease progression (#11, who then died, and #3, who was switched to BRAF targeted therapy) before the scheduled re-evaluation, response to treatment was assessed at 12 weeks after the first cycle infusion by radiographic imaging using RECIST 1.1 (week 12 response); for late response evaluation, progression was confirmed or excluded after an additional 12 weeks of treatment (best response). Disease control was defined as complete response, partial response or stable disease. Toxicity was measured according to the Common Terminology Criteria for Adverse Events v.4.0.

PBMC and plasma extraction

PBMC were isolated from blood samples using Lymphoprep (STEMCELL Technologies, Cambridge, UK) and SepMate tubes (STEMCELL Technologies, Cambridge, UK) as per manufacturer's instructions. Red cell lysis was performed with RBC Lysis Buffer (BioLegend, San Diego, CA, USA) as per manufacturer's instruction. PBMC' and sorted $CD3^+$ T cell subsets' DNA was extracted using QIAamp DNA Blood Mini kits (Qiagen, Manchester, UK) as per manufacturer's instructions.

cfDNA analyses

Extraction and quantification of cfDNA was carried out as described previously[46] for patients #11 to #27 and #29 to #39.

FACS analysis

Following isolation, PBMC for patients #1 to #50 were kept at 4°C in phosphate buffered saline plus 2% fetal bovine serum and analyzed within 24 hours. PBMC were suspended in FACS buffer (PBS containing 2% FBS, 2mM EDTA and 0.02% sodium azide) plus 50ul of Brilliant Stain Buffer (BD Biosciences, San Diego, CA, USA) and Human TruStain FcX (BioLegend, San Diego, CA, USA) as per manufacturer's instructions, and incubated at room temperature for forty minutes with T_{reg} and $T_{maturation}$ panels of fluorochrome labelled antibodies from BioLegend (San Diego, CA, USA); T_{reg} panel: CD3 (1:100, cat 317336), CD4 (1:100, cat 317438), CD8a (1:40, cat 300914), CD25 (1:10, 302610), CD127 (1:40

351304); $T_{maturation}$ panel: CD3 (1:100, cat 317337), CD4 (1:100, cat 317438), CD8a (1:40, cat 300906), CD45RA (1:100, 304130), CD45RO (1:200, 304228), CD31 (1:40, cat 303118), CD27 (1:200, 356410), CCR7 (1:20, cat 560765; BD Pharmingen, Franklin Lakes, NJ, USA). LIVE/DEAD Fixable Blue Dead Cell Stain (Thermo Fisher Scientific, Waltham, MA, US) was added to the final suspension to exclude dead cells. Stained PBMC were washed once at 300g for 7 minutes in FACS buffer and analyzed using LSR II, LSR Fortessa, Aria II or Aria III (Special Order Research Product) (BD Biosciences, Franklin Lakes, NJ, USA) cytometers and FlowJo software (v.10, Tree Star Inc., Ashland, OR, USA). $CD8^+$ T cell subsets were live-sorted with Aria III and frozen before DNA extraction.

$T_{reinvigoration}$ staining (performed for patients #1, #24, #29, #42, #54): PBMC previously frozen in FBS+10% DMSO were thawed in cold RPMI and washed twice. Then, PBMC were suspended in FACS buffer and Human TruStain FcX (BioLegend, San Diego, CA, USA) as per manufacturer's instructions, and incubated at room temperature for forty minutes with antibodies targeting CD3 (1:100, cat 317337), CD4 (1:100, cat 317438), CD8a (1:40, cat 300906), CD45RA (1:100, 304130), CD45RO (1:200, 304228), CD27 (1:200, 356410), CCR7 (1:20, cat 560765; BD Pharmingen), PD1 (1:40, cat 329939; BioLegend) and LIVE/DEAD Fixable Blue Dead Cell Stain (Thermo Fisher Scientific). Stained PBMC were then fixed and permeabilised with Perm/Fix kit according to manufacturer instructions, and stained for Ki67 (1:20, cat 350507; BioLegend) for 30 minutes at room temperature. Stained cells were resuspended in FACS buffer and analyzed using LSR Fortessa (BD Biosciences) cytometer and FlowJo software (v.10, Tree Star Inc., Ashland, OR, USA).

In patients #1, #10, #11, #12, #13, #22, #24, #25, #26, #27, #30, #42, #51-54 an aliquot of PBMC was frozen in FBS+10 % DMSO immediately after separation and then thawed and stained with CD3 fluorescent antibody as per above; $CD3^+$ cells were sorted with Aria III (BD Biosciences) and used for the TREC quantification.

T_{IE} cells were quantified as the percentage of $CD27^-/CCR7^-$ cells in the $CD3^+/CD8^+/CD45RO^+/CD45^-$ gate (Extended Data Extended Data Fig. 1). Gating strategy is shown in Extended Data Extended Data Fig. 1.

TREC

TREC analysis was performed using frozen PBMC for patients #1, #10, #11, #12, #13, #22, #24, #25, #26, #27, #30, #42, #51-54. TREC quantification was performed with droplet digital polymerase chain reaction (ddPCR) using custom TREC assay (TREC forward primer 5'-CACATCCCTTTCAACCATGCT-3' at final concentration 450nM, TREC reverse primer 5'-GCCAGCTGCAGGGTTTAGG-3' at final concentration 450nM and HEX-Black Hole probe 5'-ACACCTCTGGTTTTTGTAAAGGTGCCCACT-3' at final concentration 250nM, as per C Falci *et al.*[47], Sigma-Aldrich, Dorset, UK). For ddPCR, the TREC assay was added to 20ng DNA from sorted $CD3^+$ peripheral T cells, 11μL ddPCR Supermix for Probes (NodUTP) (Bio-rad, Hercules, CA) and 1.1μL of TERT TaqMan Copy Number Reference Assay (Thermo Fisher Scientific, Waltham, MA) in a total volume of 22μL. Droplets were generated and analyzed using the QX200 AutoDG ddPCR system according to the manufacturer's instructions (Bio-Rad, Hercules, CA, USA). Cycling conditions were 95°C for 10 minutes, followed by 40 cycles of 95°C for 15 seconds; 55°C for 1 minute;

50°C for 2 minute. To set up and optimise the assay, we used a TREC-plasmid positive control, designed as follows: TREC-plasmid forward primer 5'-AAAGAGGGCAGCCCTCTCCAAGGCAAA-3' and TREC-plasmid reverse primer 5'-AGGCTGATCTTGTCTGACATTTGCTCCG-3' as per Richardson *et al.*[48] (Sigma-Aldrich, Dorset, UK) were used to amplify the 376 bp TREC junction from healthy donor PBMC DNA. PCR amplification was performed using Quick-Load Taq 2X Master Mix (NEB, Hitchin, UK) on a Mastercycler Nexus Gradient thermal cycler (Eppendorf, Stevenage, UK). Cycling conditions were 95°C for 30 seconds, followed by 30 cycles of 95°C for 15 seconds, 60°C for 30 seconds, 68°C for 30 seconds, and 68°C for 5 minutes. The resulting amplicon was purified using the QIAquick PCR Purification Kit (Qiagen, Manchester, UK), TA cloned into the pGEM-T Easy plasmid (Promega, Southampton, UK) and transformed into competent *E. coli* strain JM109 cells prepared using the Mix & Go *E. coli* Transformation Kit (Zymo, Irvine, USA). Plasmid DNA was purified using the QIAprep Spin Miniprep Kit (Qiagen, Manchester, UK) and Sanger sequencing using the T7 5'-TAATACGACTCACTCTAGGG-3' and SP6 5-ATTTAGGTGACACTATAG-3' primers was used to confirm correct insert identity. The final plasmid was designated TREC-plasmid.

RNA sequencing

RNA was extracted from a pre-treatment human fresh frozen tumor sample for one patient with available tissue (patient #12) using AllPrep DNA/RNA kit (Qiagen, Manchester, UK) according to manufacturer's instructions. Indexed PolyA libraries were prepared using 200ng of total RNA and 14 cycles of amplification with the Agilent SureSelect Strand Specific RNA Library Prep Kit for Illumina Sequencing (Agilent, G9691B, Santa Clara, CA, US). Libraries were quantified by qPCR using the KAPA Library Quantification Kit for Illumina platforms (Kapa Biosystems Inc., KK4873, Wilmington, MA, US). Paired-end 100bp sequencing was carried out by clustering 15pM of pooled libraries on the cBot and sequenced on the Illumina HiSeq 2500 in high output mode using TruSeq SBS V3 chemistry (Illumina Inc., San Diego, CA, US). After removing adapters using Cutadapt (v1.14) and trimming poor quality base calls using Trimmomatic (v0.36)[49], the human reads were aligned to GRCh37 (release 75) using STAR (v2.5.1) aligner[50], respectively.

TCR analysis

TCR sequences were inferred from RNA Seq data from one patient for which we had a frozen pre-treatment metastasis biopsy sample using ImReP.[17]

ImmunoSEQ® TCRb Assay kit (Adaptive Biotechnologies, Seattle, WA, USA) was used to amplify and sequence TCR sequences in cfDNA and PBMC's DNA as per manufacturer's instructions. We loaded the same DNA input for all PBMC (350ng, patients #11 to #39) and cfDNA (40ng, patients #11 to #27 and #29 to #39) samples, while for the sorted T cell subsets (for patients #12, #16, #17, #18, #19, #29) we loaded all the DNA extracted from the sorted cells. A metafile will be available with each single sample and anonymous patient information. Pooled libraries were quantified by qPCR using the KAPA Library Quantification Kit for Illumina platforms (Kapa Biosystems Inc., KK4873, Wilmington, MA, US). Sequencing was carried out by clustering 0.6-1.1pM of pooled libraries on the Illumina NextSeq 500 according to Adaptive Biotechnologies' instructions. Healthy donor

PBMC TCR control data were downloaded from ImmunoSEQ® Immune ACCESS (Adaptive Biotechnologies, Seattle, WA, USA)(http://adaptivebiotech.com/pub/3d047774-29d9-441f-a71e-7725b5891b4d). TCR sequencing data were analyzed with ImmunoSEQ® ANALYZER (Adaptive Biotechnologies, Seattle, WA, USA) and R LymphoSeq package (v. 3.4.1, The R Foundation for Statistical Computing, Vienna, Austria). The clonal relatedness was calculated setting an edit distance=3 using the function *clonalRelatedness* from R package LymphoSeq. Matched paired pre-treatment and week 3 melanoma biopsy and PBMC samples of locally-advanced melanoma patients were downloaded from referenced accession Amaria *et al.*[18] (TCR sequencing data were downloaded from EGAS00001003178 EGA study accession dataset EGAD00010001608, patient clinical history metadata file from EGAD00001004352). Consecutive patients #11 to #27 from The Christie NHS Foundation Trust constituted the training cohort. The external validation data were pooled from the cohorts of patients from an independent cohort of patients from The Christie NHS Foundation Trust (patients #28 to #39), a cohort of metastatic melanoma patients from AC Huang *et al.*[7] (PBMC $CD38^+$ plus PBMC $CD38^-$ merged populations from patient #12288, #13471, #14746 and #14835; TCR sequencing data were kindly made available by the Authors) and the cohort of locally-advanced treatment naive melanoma patients from referenced accession Amaria *et al.*[18] (patients #01, #02, #04, #05, #06, #07, #08, #010, #011, #013, #015; TCR sequencing data were downloaded from EGAS00001003178 EGA study accession dataset EGAD00010001608, patient clinical history metadata file from EGAD00001004352). Gini coefficient was used as a measure of clonality[51] and calculated with the function *clonality* from LymphoSeq R package. Clonal relatedness was calculated with clonalRelatedness LymphoSeq function, and similarity was assessed by means of Bhattacharyya coefficient using bhattacharyyaMatrix LymphoSeq function. The diversity was calculated using Renyi index (α=1) as per Spreafico *et al.*[52], with time point pairwise analysis for each single patient. Linear discriminant analysis (coefficient of linear discriminants LD1: $[\Delta_{W3}\text{Renyi index}]^2$=5.2 and LD2:$[\Delta_{W3}\text{Gini coefficient}]^2$=261.3) and validation to calculate balanced accuracy were performed using R MASS and caret packages (v. 3.4.1, The R Foundation for Statistical Computing, Vienna, Austria). For further details refer to the Extended R scripts that are available on GitLab (https://gitlab.com/cruk-mi/tcell-immune-awakening).

CyTOF surface phenotype analysis

Differential marker expression analysis was performed on CyTOF (cytometry by time-of-flight mass spectrometry) data from Krieg *et al.*[8] and Greenplate *et al.*[24] downloaded from a publicly available repository (referenced accession https://flowrepository.org/experiments/1124 and http://flowrepository.org/id/FR-FCM-ZZMC), using the custom workflow described in Nowicka *et al.*[53]. All analyses on CyTOF data were performed after arcsinh (with cofactor=5) transformation of marker expression and correction for batch effect (function removeBatchEffect from limma R package). The T_{IE} subset was identified by differential expression of T lymphocytic markers CD3, CD8a, CD45RA CD45RO, CCR7 and CD27. Cell populations clustering was obtained with R package FlowSOM after the metaclustering step (ConsensusClusterPlus R package).

REAP-Seq single cell analysis

Differential proteomic and RNA expression analysis was performed on REAP-Seq data from Peterson *et al.*[27] downloaded from a publicly available repository (referenced accession https://www.ncbi.nlm.nih.gov/geo/query/acc.cgi?acc=GSE100501), using R package Seurat v.2.4.0[54]. The single cells with T_{IE} phenotype were identified based on the expression level of antibody derived tags (ADT) CD8a, CD45RA, CD45RO, CD27 and CD197 (CCR7) (FetchData command with set conditions based on the expression level, cut-offs for positive/negative and high/low have been set based on the normalized data), and the cell identities have been used to define the T_{IE} cluster (SetIdent command). The cell differential expression analysis in the T_{IE} from PBMC vs after *in vitro* stimulation was performed with the function FindMarkers in the combined Seurat object (RunCCA). The ADT data Seurat matrices were imported in Cytobank[55] to analyze the differential representation of the $CD8^+$ subsets under different experimental conditions.

Statistics and Reproducibility

Unless otherwise stated, all statistical tests were two-tailed. The statistical differences between two groups for numerical variables were assessed using two-tailed Mann-Whitney U test (unpaired comparisons) or Wilcoxon test (paired comparisons). The statistical differences between multiple, paired measures was assessed using Friedman test. Deltas were calculated as the difference between W3 and T0 values. The statistical differences of categorical variables between groups were assessed using two-tailed Chi-square or Fisher's exact test, according to group dimension. Correlation between continuous variables was assessed with Spearman test (independent variables) or with linear regression (dependent variables). Kaplan-Meier plots with the log-rank test (3 week landmark analysis) were used to analyze survival data. Univariate Cox regression was used to calculate the hazard of death. P values<0.05 were retained as significant, Cox-Snell residuals were used to verify the proportional hazard hypothesis (P=0.141, with a P value>0.05 confirming the hypothesis). Sample size calculation was performed using G*Power software (Erdfelder, Faul, & Buchner, 1996), using the effect size and standard deviation. For the comparison of ΔRES in peripheral blood mononuclear cells vs cfDNA in patients with disease response sample size was 14 for alpha=0.05 and 1-beta=0.8. For the linear discriminant analysis we used the power and sample size calculation for linear regression with 2 covariates and effect size f^2=0.55, and total sample size was calculated=17 for alpha=0.05 and 1-beta=0.8. For the T cell subset analyses for the immune-effector T cells in patients with progression vs disease control the total sample size was 32 for alpha=0.05 and 1-b=0.8. No data were excluded from the analyses. The Investigators were blinded during experiments; outcome assessment was performed after experiments. Analyses were performed with GraphPad Prism version 7 (GraphPad Software, La Jolla California USA) or R (v. 3.4.1, The R Foundation for Statistical Computing, Vienna, Austria). Further information on research design is available in the Nature Research Reporting Summary linked to this article.

Extended Data

Europe PMC Funders Author Manuscripts

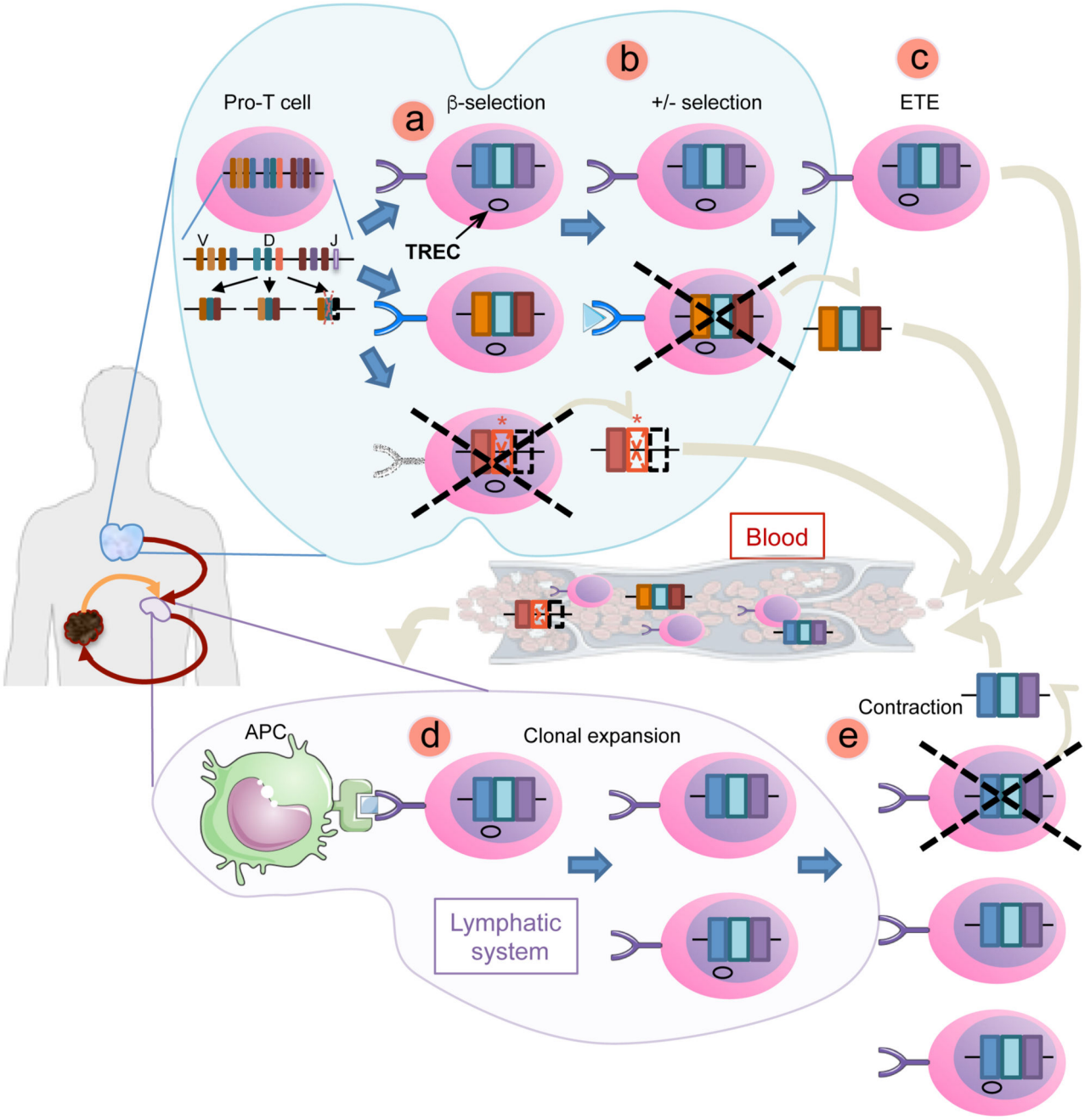

Extended Data Fig. 1. Schematic summarizing T cell maturation and life-cycle.

a Pro-T cells undergo sequential somatic recombination of their T cell Receptor β (*TCR*) loci in attempts to generate functional TCR with unique CDR3 antigen binding regions. Cells that fail to generate a functional TCRβ at the first attempt can recombine their second *TCR* allele, but cells which fail to produce a functional TCR at the end of the process (crossed red box) are eliminated (β-selection) and their DNA, which encodes the *CDR3* unique regions, enters the blood as circulating cell-free DNA (cfDNA). Surviving cells retain the T cell receptor excision circle (TREC) generated during *TCR* locus rearrangement

as an episome in the nucleus. The TREC does not replicate so is diluted during subsequent cell divisions. **b** T cells with a functional TCR undergo positive and negative selection (+/- selection) for HLA and self-antigen recognition. The *CDR3* DNA from T cells eliminated during this step is released into the blood. **c** Naive T cells enter the circulation as early thymic emigrants (ETE). **d** T cells primed by antigen presenting cells (APC) in the lymphatic system undergo clonal expansion, which dilutes the TREC amongst the daughter cells. **e** T cell homeostasis is maintained by subsequent contraction (turnover cycles), releasing further *CDR3* DNA into the blood.

Europe PMC Funders Author Manuscripts

Europe PMC Funders Author Manuscripts

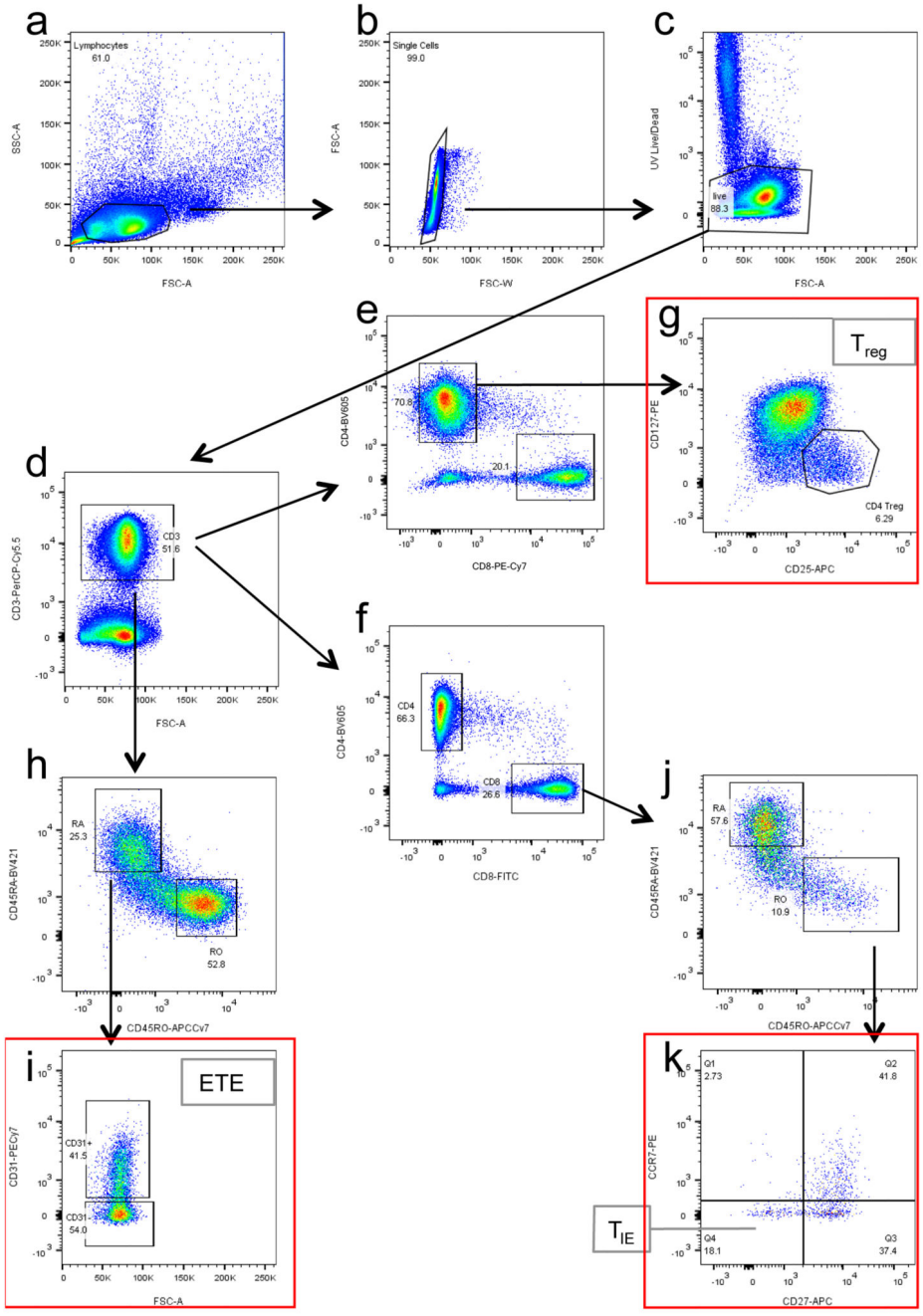

Extended Data Fig. 2. Gating strategy for the identification of T cell subsets in peripheral blood of melanoma patients.

Multiparametric fluorescence activated cell sorting analysis using the indicated gates. **a** Lymphocyte gate on side scatter/forward scatter; **b** single cell gate to exclude doublets; **c** live gating to exclude dead cells from subsequent gates; **d** $CD3^+$ gate for T cells; **e,f** $CD4^+$ and CD8+ gates for “helper” and “killer” T cell subsets, CD8 was detected with a PE-Cy7 labelled antibody for the T_{reg} panel (**e**) and with a FITC labelled antibody for the T maturation panel (**f**); **g** $CD4^+/CD25^+/CD127^{-/low}$ regulatory T cells (T_{reg}); **h** naive (top left)

and memory (bottom right) gates total T cells; **i** ETE (top) and CD31-naive (bottom) gates for naive T cells; **j** naive (top left) and memory (bottom right) gates for $CD8^+$ T cells; **k** $CD8^+$ memory T cell subsets, the left bottom subset ($CCR7^-/CD27^-$) represents the T_{IE} cells.

Europe PMC Funders Author Manuscripts

Europe PMC Funders Author Manuscripts

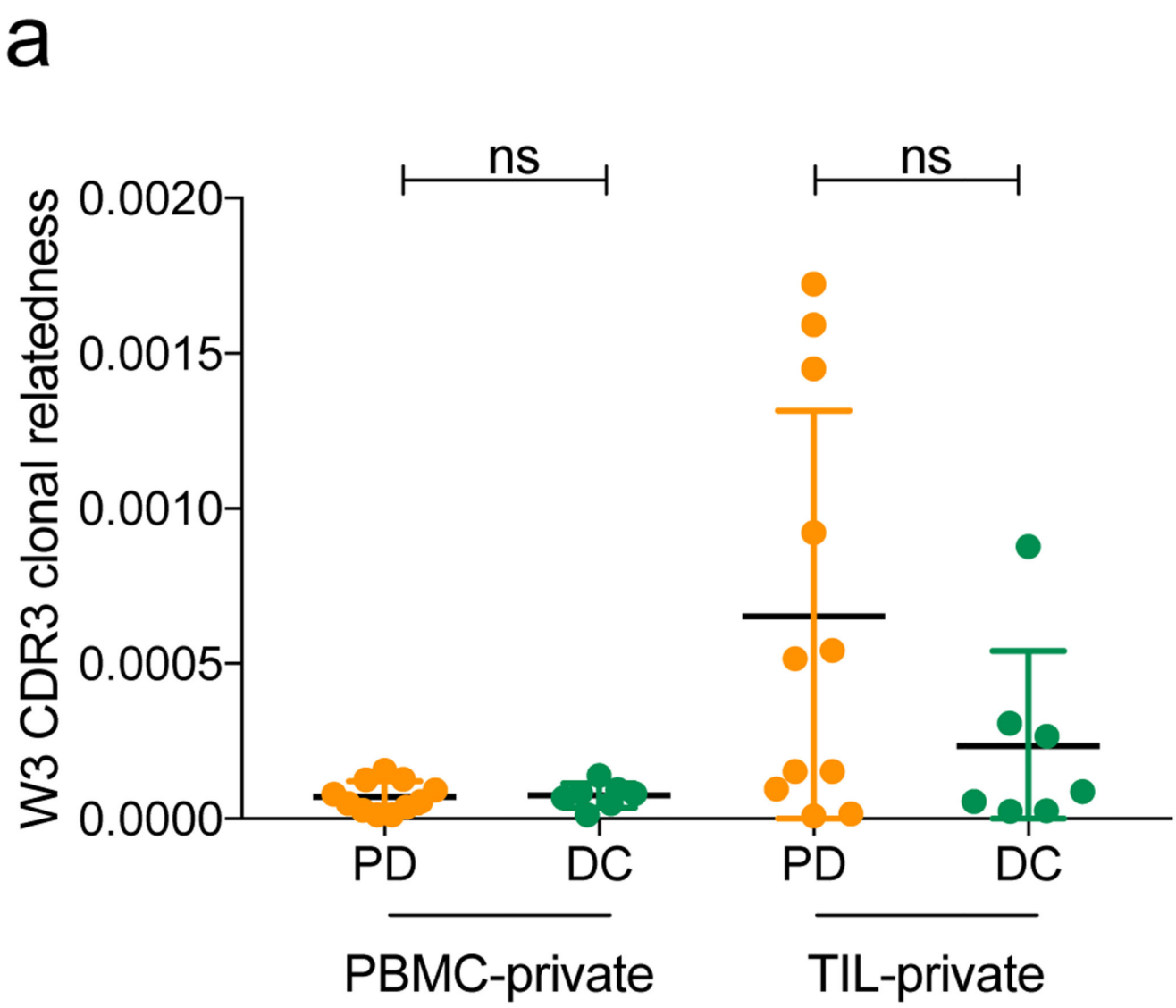

Extended Data Fig. 3. Clonal relatedness in tumor infiltrating T cells and PBMC.

a Clonal relatedness changes in PBMC-private and TIL-private *TCR* pools; comparison of week 3 (W3) *CDR3* clonal relatedness in patients with progressive disease (PD, n=11 patients) and disease control at week 12 (DC, n=7 patients) in the PBMC-private (P=0.724, median=$0.6x10^{-6}$ and $0.6x10^{-6}$, respectively; two-sided Mann-Whitney U test) and TIL-private pools (P=0.246, median= $0.5x10^{-4}$ and $0.8x10^{-5}$, respectively; two-sided Mann-Whitney U test). Dot represents one patient; green indicates DC; orange indicates PD; error bar is standard deviation.

Europe PMC Funders Author Manuscripts

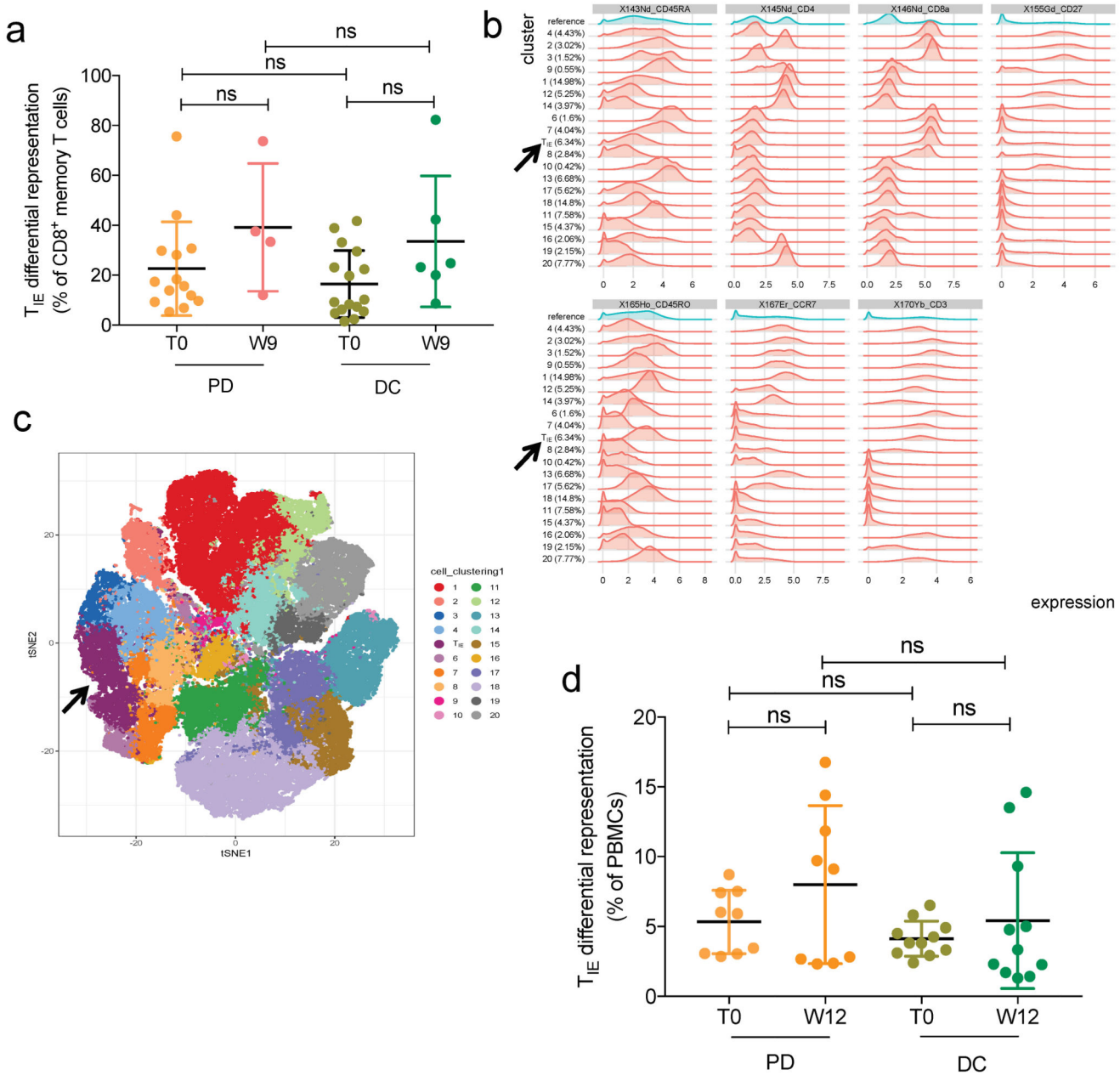

Extended Data Fig. 4. Identification of T_{IE} in CPI-treated patient PBMC.

a Comparison of differential abundance of T_{IE} in $CD8^+$ memory T cells in the PBMC of The Christie NHS Foundation Trust patients with best response progressive disease (PD, orange, n=14) and disease control (DC, green, n=16) at T0 (n=30, light shade) and week 9 (W9; n=10, dark shade; PD, n=4, DC, n=6). Differences over time were not significant for PD (median=15.2 and 35.5; P=0.375; two-sided Wilcoxon test) or DC (median=7.9 and 24; P=0.219; two-sided Wilcoxon test); PD vs DC patient values did not differ at T0 (P=0.275; two-sided Mann-Whitney U test) or W9 (P=0.762; two-sided Mann-Whitney U test). **b** Distributions of marker intensities of the T cell surface markers in the 20 cell populations (clusters) for PBMC from a published cohort[3] (n=20 patients). Cluster 5 was identified as

the T_{IE} subset. Blue densities are calculated over all the cells and serve as a reference and red densities represent marker expression for cells in a given cluster. Arrows highlight the T_{IE} subset. **c** T-stochastic neighbor embedding of single cell profiles (dots) performed in an external cohort[3] using the T cell surface markers CD3, CD4, CD8, CD45RA, CD45RO, CCR7 and CD27; different colors are attributed by clustering. Arrow highlights the T_{IE} subset. **d** Comparison of the differential abundance of the T_{IE} cluster in the PBMC from a published cohort[3] of patients with PD (orange, n=9) or DC (green, n=11) at pre-treatment (light shade, n=20; PD, n=9; DC, n=11) and at week 12 (W12, dark shade, n=20) on treatment with pembrolizumab or nivolumab in the external cohort. Horizontal bars indicate the differences over time for the PD (median at T0=5.9 and W12=9.1; P=0.164; two-sided Wilcoxon test) or DC patients (median at T0=3.8 and W12=3.3; P=0.831; two-sided Wilcoxon test), and difference in the two response groups at T0 or W12 (P=0.37 and P=0.201, respectively; two-sided Mann-Whitney U test). Light and dark orange indicate PD for T0 and W9-W12, respectively, light and dark green indicate DC for T0 and W9-W12, respectively; n represents patients; ns means not significant P values; error bars are standard deviation.

Europe PMC Funders Author Manuscripts

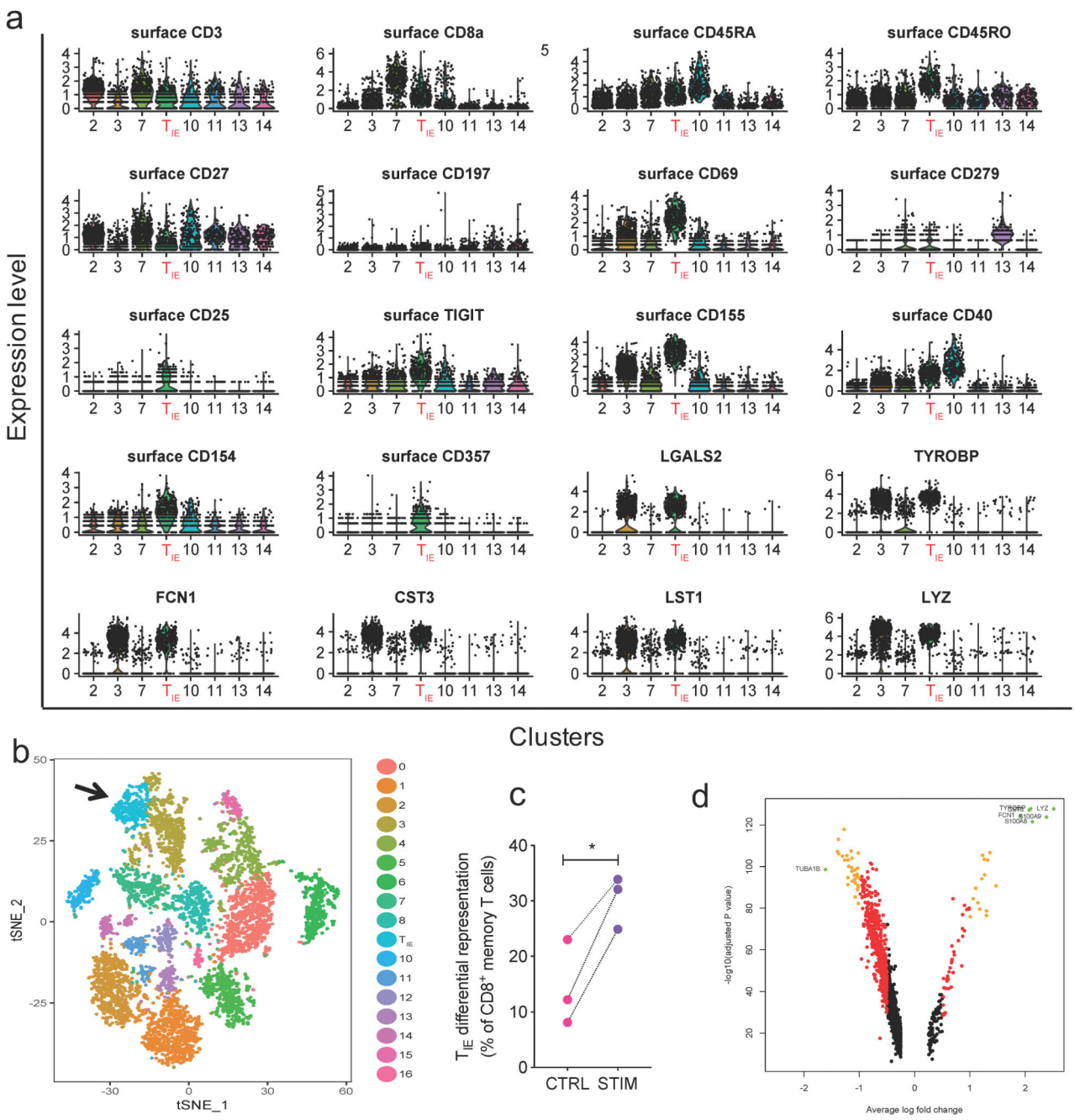

Extended Data Fig. 5. Characterization of T_{IE} in PBMC.

Analysis of published cohort of PBMC single cell data from reference #27. **a** Violin plots of the expression level of selected phenotypic and transcriptomic features of the clusters identifying peripheral T cell subsets (n=7488 single cells), the cluster with T_{IE} phenotype is indicated in red; the plots represent the density probability, the area shapes reflect the data distribution; horizontal lines represent the minima and maxima values; central dots represent the medians. Overall minima, mean and maxima values: surface CD3=0, 0.3785, 4.1396; surface CD8a=0, 0.96327, 6.21476; surface CD45RA=0, 0.8161, 4.8508; surface

Europe PMC Funders Author Manuscripts

CD45RO=0, 0.6628, 4.6468; surface CD197/CCR7=0, 0.8961, 5.7975; surface CD69=0, 0.5219, 4.2200; surface CD279=0, 0.09787, 3.84886; surface CD25=0, 0.08653, 4.00428; surface TIGIT=0, 0.4663, 4.2381; surface CD155=0, 0.4850, 4.6679; surface CD40=0, 0.6003, 5.5083; surface CD154=0, 0.4062, 3.8159; surface CD357=0, 0.1193, 4.0316; LGALS2=0, 0.561, 6.089; TYROBP=0, 1.337, 6.662; FCN1=0, 1.290, 6.789; CST3=0, 1.404, 6.504; LST1=0, 1.042, 6.097; LYZ=0, 1.775, 6.859. **b** T-SNE plot showing the clusters identified by means of the antibody derived tags (ADT) targeted to surface markers (n=7488 single cells); the black arrow indicates the cluster with T_{IE} phenotype. **c** Plot showing the proportion of cells with the T_{IE} phenotype from the same published cohort after standard *in vitro* culture (CTRL, n=3 sorted healthy donor peripheral blood $CD8^+$ naïve T cell samples in standard culture) or following stimulation with anti-CD3/anti-CD27 Dynabeads[23] (STIM, n=3 sorted healthy donor peripheral blood $CD8^+$ naïve T cell samples after stimulation) (P=0.0267, two-sided paired t test, two degrees of freedom) and **d** Volcano plot representing the transcriptomic differential expression of the cells with the T_{IE} phenotype in PBMC presented in **a** (n=7488 single cells) or expanded from naive $CD8^+$ T cells from the experiment presented in **c**[22] (n=12217 single cells; two-sided Wilcoxon test with Bonferroni correction for multiple comparisons).

Europe PMC Funders Author Manuscripts

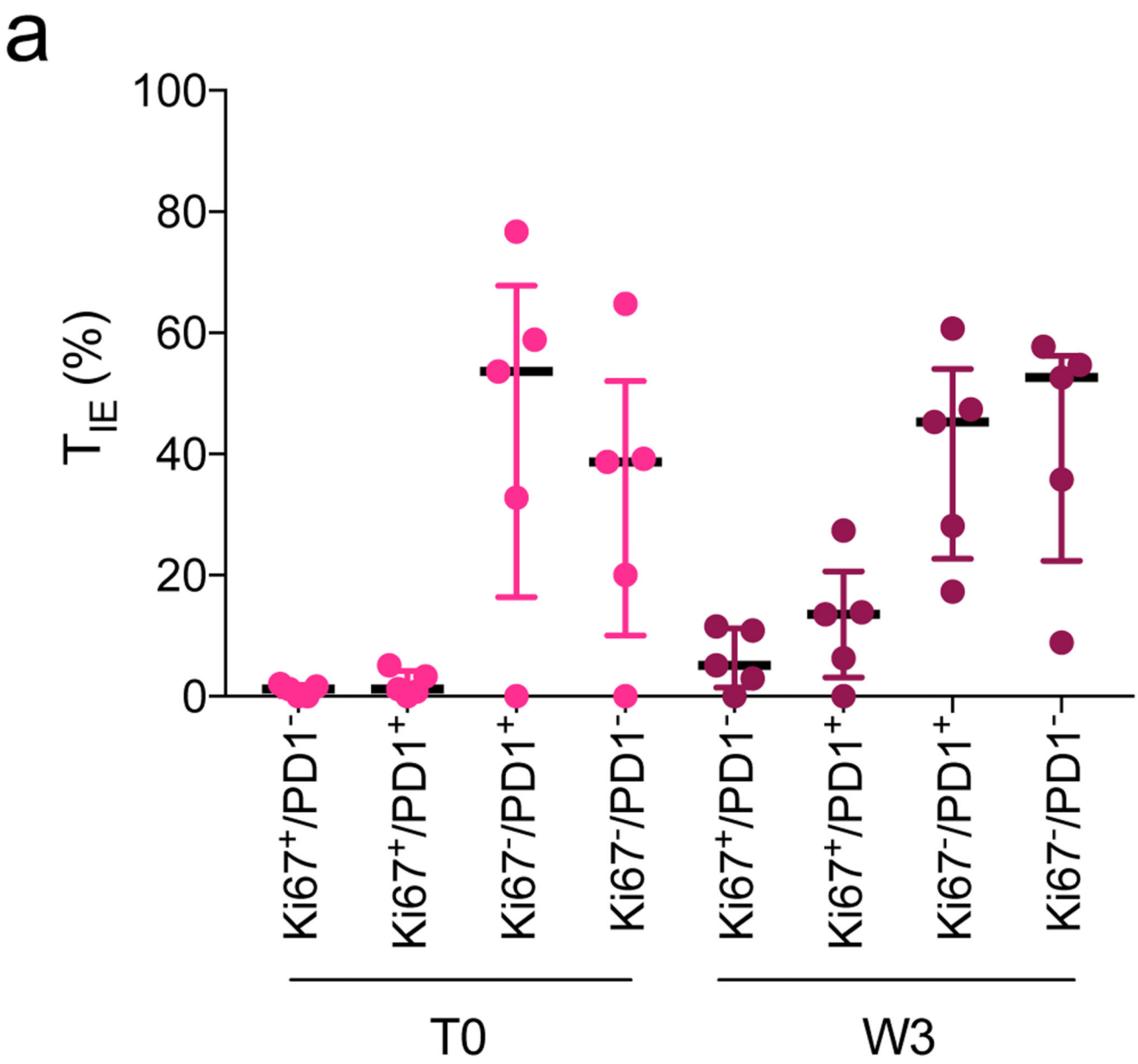

Extended Data Fig. 6. Expression of Ki-67 and PD-1 in peripheral T_{IE} cells before and after 1 cycle of CPI.

a Expression of Ki67 and PD1 in the T_{IE} subset as measured by FACS in n=5 frozen samples of PBMC from The Christie NHS Foundation Trust metastatic melanoma patients treated with CPI, at pre-treatment (T0) and after 1 cycle of CPI (W3); horizontal line indicates median; error bar indicates standard deviation. The small sample size did not allow statistical comparison of the outcome groups.

Supplementary Material

Refer to Web version on PubMed Central for supplementary material.

Acknowledgments

We are grateful to the patients who participated to this study and their families. We thank Dr. Patricio Serra-Bellver for his help in the collection of the patient samples, Ruth Cox for her assistance with graphics preparation, and Prof. Judi Allen, Dr. Santiago Zelenay and the Molecular Oncology Group for their advice. We thank Dr. Gillian Williams for her assistance during the TCR sequencing. This work was supported by CRUK (A27412 and A22902), the Harry J Lloyd Charitable Trust (Career Development Award for SV) and the Wellcome Trust (100282/Z/12/Z). The role of the MCRC Biobank is to distribute samples and therefore, cannot endorse studies performed or the interpretation of results.

References

1. Badovinac VP, Porter BB, Harty JT. Programmed contraction of CD8(+) T cells after infection. Nat Immunol. 2002; 3:619–626. DOI: 10.1038/ni804 [PubMed: 12055624]
2. Ugurel S, et al. Survival of patients with advanced metastatic melanoma: the impact of novel therapies-update 2017. Eur J Cancer. 2017; 83:247–257. DOI: 10.1016/j.ejca.2017.06.028 [PubMed: 28756137]
3. Wykes MN, Lewin SR. Immune checkpoint blockade in infectious diseases. Nat Rev Immunol. 2018; 18:91–104. DOI: 10.1038/nri.2017.112 [PubMed: 28990586]
4. Goldszmid RS, Dzutsev A, Trinchieri G. Host immune response to infection and cancer: unexpected commonalities. Cell Host Microbe. 2014; 15:295–305. DOI: 10.1016/j.chom.2014.02.003 [PubMed: 24629336]
5. Vance RE, Eichberg MJ, Portnoy DA, Raulet DH. Listening to each other: Infectious disease and cancer immunology. Sci Immunol. 2017; 2doi: 10.1126/sciimmunol.aai9339
6. Dunn GP, Old LJ, Schreiber RD. The three Es of cancer immunoediting. Annu Rev Immunol. 2004; 22:329–360. DOI: 10.1146/annurev.immunol.22.012703.104803 [PubMed: 15032581]
7. Huang AC, et al. T-cell invigoration to tumour burden ratio associated with anti-PD-1 response. Nature. 2017; 545:60–65. DOI: 10.1038/nature22079 [PubMed: 28397821]
8. Krieg C, et al. High-dimensional single-cell analysis predicts response to anti-PD-1 immunotherapy. Nat Med. 2018; 24:144–153. DOI: 10.1038/nm.4466 [PubMed: 29309059]
9. Jacquelot N, et al. Predictors of responses to immune checkpoint blockade in advanced melanoma. Nat Commun. 2017; 8doi: 10.1038/s41467-017-00608-2
10. Huang AC, et al. A single dose of neoadjuvant PD-1 blockade predicts clinical outcomes in resectable melanoma. Nat Med. 2019; 25:454–461. DOI: 10.1038/s41591-019-0357-y [PubMed: 30804515]
11. Hozumi N, Tonegawa S. Evidence for somatic rearrangement of immunoglobulin genes coding for variable and constant regions. Proc Natl Acad Sci U S A. 1976; 73:3628–3632. [PubMed: 824647]
12. Schatz DG, Baltimore D. Uncovering the V(D)J recombinase. Cell. 2004; 116
13. Janeway, CA, , JrT, P, Walport, M. , et al. Immunobiology: The Immune System in Health and Disease. 5th edition. Garland Science; 2001.
14. Kohler S, Thiel A. Life after the thymus: CD31+ and CD31- human naive CD4+ T-cell subsets. Blood. 2009; 113:769–774. DOI: 10.1182/blood-2008-02-139154 [PubMed: 18583570]
15. Steinmann GG, Klaus B, Muller-Hermelink HK. The involution of the ageing human thymic epithelium is independent of puberty. A morphometric study. Scand J Immunol. 1985; 22:563–575. [PubMed: 4081647]
16. Geenen V, et al. Quantification of T cell receptor rearrangement excision circles to estimate thymic function: an important new tool for endocrine-immune physiology. J Endocrinol. 2003; 176:305–311. [PubMed: 12630915]
17. Mangul SMI, Yang HT, Strauli N, Montoya D, Rotman J, Van Der Wey W, Ronas JR, Statz B, Zelikovsky A, Spreafico R. Profiling adaptive immune repertoires across multiple human tissues by RNA Sequencing. bioRxiv. 2016
18. Amaria RN, et al. Neoadjuvant immune checkpoint blockade in high-risk resectable melanoma. Nat Med. 2018; 24:1649–1654. DOI: 10.1038/s41591-018-0197-1 [PubMed: 30297909]

19. Coffey D. LymphoSeq: Analyze high-throughput sequencing of T and B cell receptors. R package version 1.4.1. 2017
20. Alves Sousa AP, et al. Comprehensive Analysis of TCR-beta Repertoire in Patients with Neurological Immune-mediated Disorders. Sci Rep. 2019; 9doi: 10.1038/s41598-018-36274-7
21. Radziewicz H, Uebelhoer L, Bengsch B, Grakoui A. Memory CD8+ T cell differentiation in viral infection: a cell for all seasons. World J Gastroenterol. 2007; 13:4848–4857. DOI: 10.3748/wjg.v13.i36.4848 [PubMed: 17828816]
22. Mahnke YD, Brodie TM, Sallusto F, Roederer M, Lugli E. The who's who of T-cell differentiation: human memory T-cell subsets. Eur J Immunol. 2013; 43:2797–2809. DOI: 10.1002/eji.201343751 [PubMed: 24258910]
23. Ribas A, et al. PD-1 Blockade Expands Intratumoral Memory T Cells. Cancer Immunol Res. 2016; 4:194–203. DOI: 10.1158/2326-6066.CIR-15-0210 [PubMed: 26787823]
24. Greenplate AR, et al. Computational Immune Monitoring Reveals Abnormal Double-Negative T Cells Present across Human Tumor Types. Cancer Immunol Res. 2019; 7:86–99. DOI: 10.1158/2326-6066.CIR-17-0692 [PubMed: 30413431]
25. Gremel G, et al. Distinct subclonal tumour responses to therapy revealed by circulating cell-free DNA. Ann Oncol. 2016; 27:1959–1965. DOI: 10.1093/annonc/mdw278 [PubMed: 27502704]
26. Robert C, et al. Nivolumab in previously untreated melanoma without BRAF mutation. N Engl J Med. 2015; 372:320–330. DOI: 10.1056/NEJMoa1412082 [PubMed: 25399552]
27. Peterson VM, et al. Multiplexed quantification of proteins and transcripts in single cells. Nat Biotechnol. 2017; 35:936–939. DOI: 10.1038/nbt.3973 [PubMed: 28854175]
28. Venken K, et al. Natural naive CD4+CD25+CD127low regulatory T cell (Treg) development and function are disturbed in multiple sclerosis patients: recovery of memory Treg homeostasis during disease progression. J Immunol. 2008; 180:6411–6420. [PubMed: 18424765]
29. Herati RS, et al. Successive annual influenza vaccination induces a recurrent oligoclonotypic memory response in circulating T follicular helper cells. Sci Immunol. 2017; 2doi: 10.1126/sciimmunol.aag2152
30. DeWitt WS, et al. Dynamics of the cytotoxic T cell response to a model of acute viral infection. J Virol. 2015; 89:4517–4526. DOI: 10.1128/JVI.03474-14 [PubMed: 25653453]
31. Amaria RN, et al. Neoadjuvant immune checkpoint blockade in high-risk resectable melanoma. Nat Med. 2018; doi: 10.1038/s41591-018-0197-1
32. Martin MD, Badovinac VP. Defining Memory CD8 T Cell. Front Immunol. 2018; 9:2692.doi: 10.3389/fimmu.2018.02692 [PubMed: 30515169]
33. Tomiyama H, Takata H, Matsuda T, Takiguchi M. Phenotypic classification of human CD8+ T cells reflecting their function: inverse correlation between quantitative expression of CD27 and cytotoxic effector function. Eur J Immunol. 2004; 34:999–1010. DOI: 10.1002/eji.200324478 [PubMed: 15048710]
34. Rossi JF, Ceballos P, Lu ZY. Immune precision medicine for cancer: a novel insight based on the efficiency of immune effector cells. Cancer Commun (Lond). 2019; 39:34.doi: 10.1186/s40880-019-0379-3 [PubMed: 31200766]
35. Yost KE, et al. Clonal replacement of tumor-specific T cells following PD-1 blockade. Nat Med. 2019; 25:1251–1259. DOI: 10.1038/s41591-019-0522-3 [PubMed: 31359002]
36. Cha E, et al. Improved survival with T cell clonotype stability after anti-CTLA-4 treatment in cancer patients. Sci Transl Med. 2014; 6doi: 10.1126/scitranslmed.3008211
37. Robert L, et al. CTLA4 blockade broadens the peripheral T-cell receptor repertoire. Clin Cancer Res. 2014; 20:2424–2432. DOI: 10.1158/1078-0432.CCR-13-2648 [PubMed: 24583799]
38. Wieland A, et al. T cell receptor sequencing of activated CD8 T cells in the blood identifies tumor-infiltrating clones that expand after PD-1 therapy and radiation in a melanoma patient. Cancer Immunol Immunother. 2018; 67:1767–1776. DOI: 10.1007/s00262-018-2228-7 [PubMed: 30167863]
39. Wei SC, et al. Distinct Cellular Mechanisms Underlie Anti-CTLA-4 and Anti-PD-1 Checkpoint Blockade. Cell. 2017; 170:1120–1133 e1117. DOI: 10.1016/j.cell.2017.07.024 [PubMed: 28803728]

40. Fritsch RD, et al. Stepwise differentiation of CD4 memory T cells defined by expression of CCR7 and CD27. J Immunol. 2005; 175:6489–6497. [PubMed: 16272303]
41. Hendriks J, Xiao Y, Borst J. CD27 promotes survival of activated T cells and complements CD28 in generation and establishment of the effector T cell pool. J Exp Med. 2003; 198:1369–1380. DOI: 10.1084/jem.20030916 [PubMed: 14581610]
42. Britschgi MR, Link A, Lissandrin TK, Luther SA. Dynamic modulation of CCR7 expression and function on naive T lymphocytes in vivo. J Immunol. 2008; 181:7681–7688. [PubMed: 19017956]
43. Larbi A, Fulop T. From "truly naive" to "exhausted senescent" T cells: when markers predict functionality. Cytometry A. 2014; 85:25–35. DOI: 10.1002/cyto.a.22351 [PubMed: 24124072]
44. Sallusto F, et al. Switch in chemokine receptor expression upon TCR stimulation reveals novel homing potential for recently activated T cells. Eur J Immunol. 1999; 29:2037–2045. DOI: 10.1002/(SICI)1521-4141(199906)29:06<2037::AID-IMMU2037>3.0.CO;2-V [PubMed: 10382767]
45. Geginat J, Lanzavecchia A, Sallusto F. Proliferation and differentiation potential of human CD8+ memory T-cell subsets in response to antigen or homeostatic cytokines. Blood. 2003; 101:4260–4266. DOI: 10.1182/blood-2002-11-3577 [PubMed: 12576317]
46. Valpione S, et al. Plasma total cell-free DNA (cfDNA) is a surrogate biomarker for tumour burden and a prognostic biomarker for survival in metastatic melanoma patients. Eur J Cancer. 2018; 88:1–9. DOI: 10.1016/j.ejca.2017.10.029 [PubMed: 29175734]
47. Falci C, et al. Immune senescence and cancer in elderly patients: results from an exploratory study. Exp Gerontol. 2013; 48:1436–1442. DOI: 10.1016/j.exger.2013.09.011 [PubMed: 24120567]
48. Richardson MW, et al. Analysis of telomere length and thymic output in fast and slow/non-progressors with HIV infection. Biomed Pharmacother. 2000; 54:21–31. [PubMed: 10721459]
49. Bolger AM, Lohse M, Usadel B. Trimmomatic: a flexible trimmer for Illumina sequence data. Bioinformatics. 2014; 30:2114–2120. DOI: 10.1093/bioinformatics/btu170 [PubMed: 24695404]
50. Dobin A, et al. STAR: ultrafast universal RNA-seq aligner. Bioinformatics. 2013; 29:15–21. DOI: 10.1093/bioinformatics/bts635 [PubMed: 23104886]
51. Thapa DR, et al. Longitudinal analysis of peripheral blood T cell receptor diversity in patients with systemic lupus erythematosus by next-generation sequencing. Arthritis Res Ther. 2015; 17:132.doi: 10.1186/s13075-015-0655-9 [PubMed: 26001779]
52. Spreafico R, et al. A circulating reservoir of pathogenic-like CD4+ T cells shares a genetic and phenotypic signature with the inflamed synovial micro-environment. Ann Rheum Dis. 2016; 75:459–465. DOI: 10.1136/annrheumdis-2014-206226 [PubMed: 25498120]
53. Nowicka M, et al. CyTOF workflow: differential discovery in high-throughput high-dimensional cytometry datasets. F1000Res. 2017; 6:748.doi: 10.12688/f1000research.11622.2 [PubMed: 28663787]
54. Gribov A, et al. SEURAT: visual analytics for the integrated analysis of microarray data. BMC Med Genomics. 2010; 3:21.doi: 10.1186/1755-8794-3-21 [PubMed: 20525257]
55. Kotecha N, Krutzik PO, Irish JM. Web-based analysis and publication of flow cytometry experiments. Curr Protoc Cytom. 2010; Chapter 10:Unit10–17. DOI: 10.1002/0471142956.cy1017s53

Europe PMC Funders Author Manuscripts

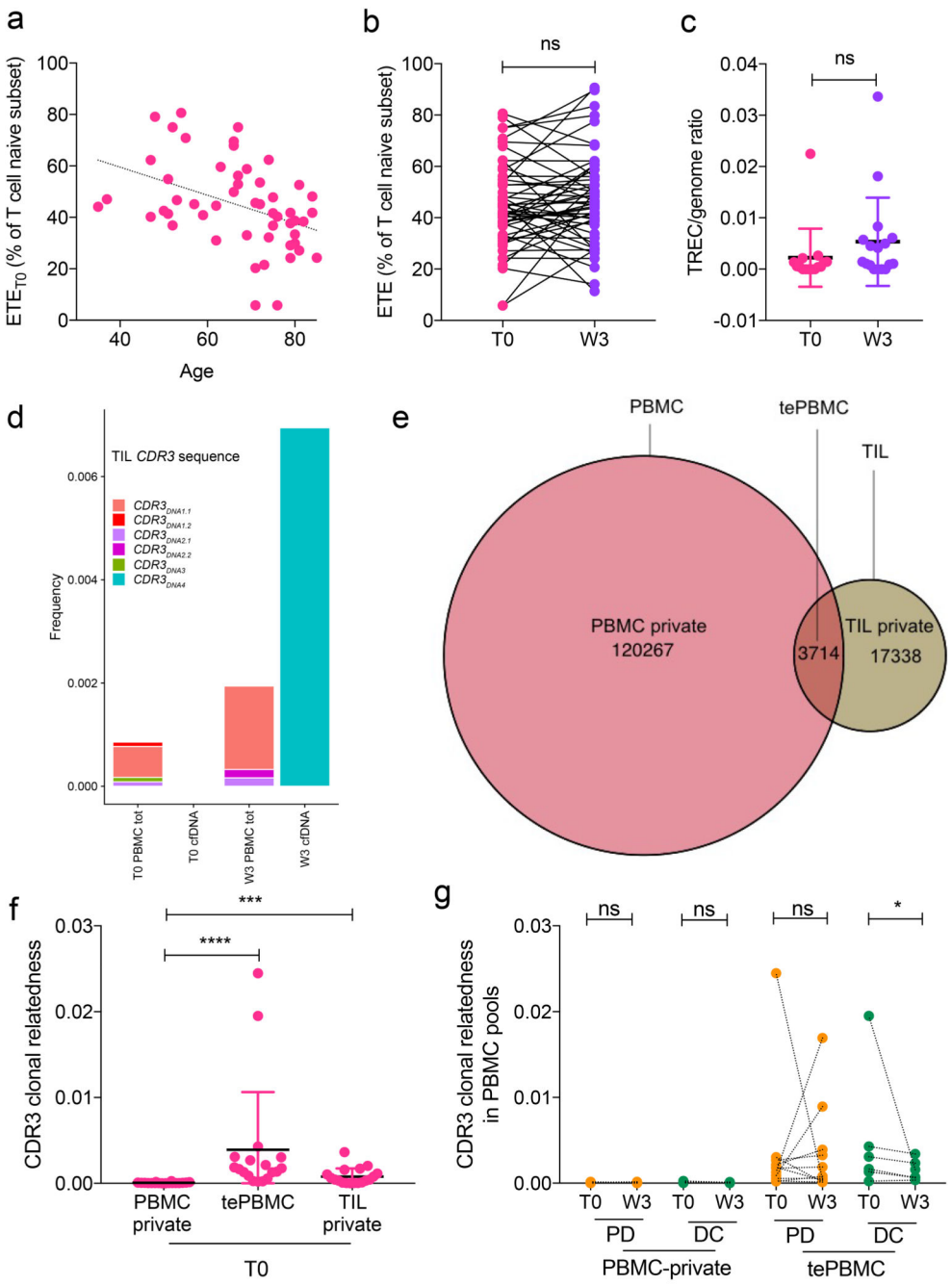

Figure 1. CPI induced peripheral TCR repertoire divergence.

a Graph showing early thymic emigrants in pre-treated patients' blood (% ETE_{T0} relative to total naive T cells; determined by FACS) relative to age (P=0.002, linear regression R^2=-0.17; n=50). **b** Levels of ETE in pre-treatment (T0) and week 3 (W3) of CPI in paired patient samples (P=0.274, two-sided Wilcoxon test, n=50). **c** TREC (T cell receptor excision circle) concentration relative to genomic DNA was measured by droplet digital PCR in sorted $CD3^+$ peripheral T cells at T0 (median $0.5x10^{-3}$) and W3 (median $0.1x10^{-2}$)(P=0.129, two-sided Wilcoxon test, n=17). **d** Tumor infiltrating T lymphocyte (TIL) *CDR3* sequences

Europe PMC Funders Author Manuscripts

also present in peripheral PBMC and cfDNA for one patient at T0 and W3. See Table 1 for specific DNA sequence; tot = total. **e** Venn diagram showing unique predicted productive *CDR3* sequences in PBMC and TIL for patient #01 at T0 (Supplementary Table 1)[18]. Numbers show unique nucleotide sequence counts for PBMC-private (pink), TIL-private (brown) and tePBMC (tumor emigrant PBMC; intersection, orange) pools. **f** Clonal relatedness (the proportion of amino acids sequences that are related by maximum edit distance=3) for CDR3 in the PBMC-private pool, tePBMC and TIL-private pools at T0. Horizontal lines: comparison of clonal relatedness between PBMC-private and TIL-private TCR sequences at T0; ***: P=0.003; n=18, two-sided Wilcoxon test; median=$0.4x10^{-6}$ and $0.4x10^{-3}$, respectively; ****: P<0.0001; n=18, two-sided Wilcoxon test; median=$0.4x10^{-6}$ and $0.2x10^{-2}$, respectively. **g** Clonal relatedness (maximum edit distance=3 amino acids) for CDR3 sequence in PBMC TCR pools at T0 and W3. Comparison between the clonal relatedness of PBMC-private TCR of patients with progressive disease (PD, orange, n=11, median=$4.3x10^{-5}$ and $5.6x10^{-5}$, respectively) or disease control (DC, green, n=7, median=$4.0x10^{-5}$ and $8.0x10^{-5}$, respectively) after 12 weeks of treatment; ns: not significant (P=0.413 and P=0.999, two-sided Wilcoxon test) and between the clonal relatedness of tePBMC TCR of patients with PD (n=11) or DC (n=7); ns: not significant (P=0.638; two-sided Wilcoxon test; median=0.002 and 0.0008, respectively); *: P=0.031; n=7, two-sided Wilcoxon test; median=0.0017 and 0.0007, respectively). Dot is one patient; line is median; error bar is standard deviation; connecting line is paired samples; ns indicates not significant P values, n represents patients.

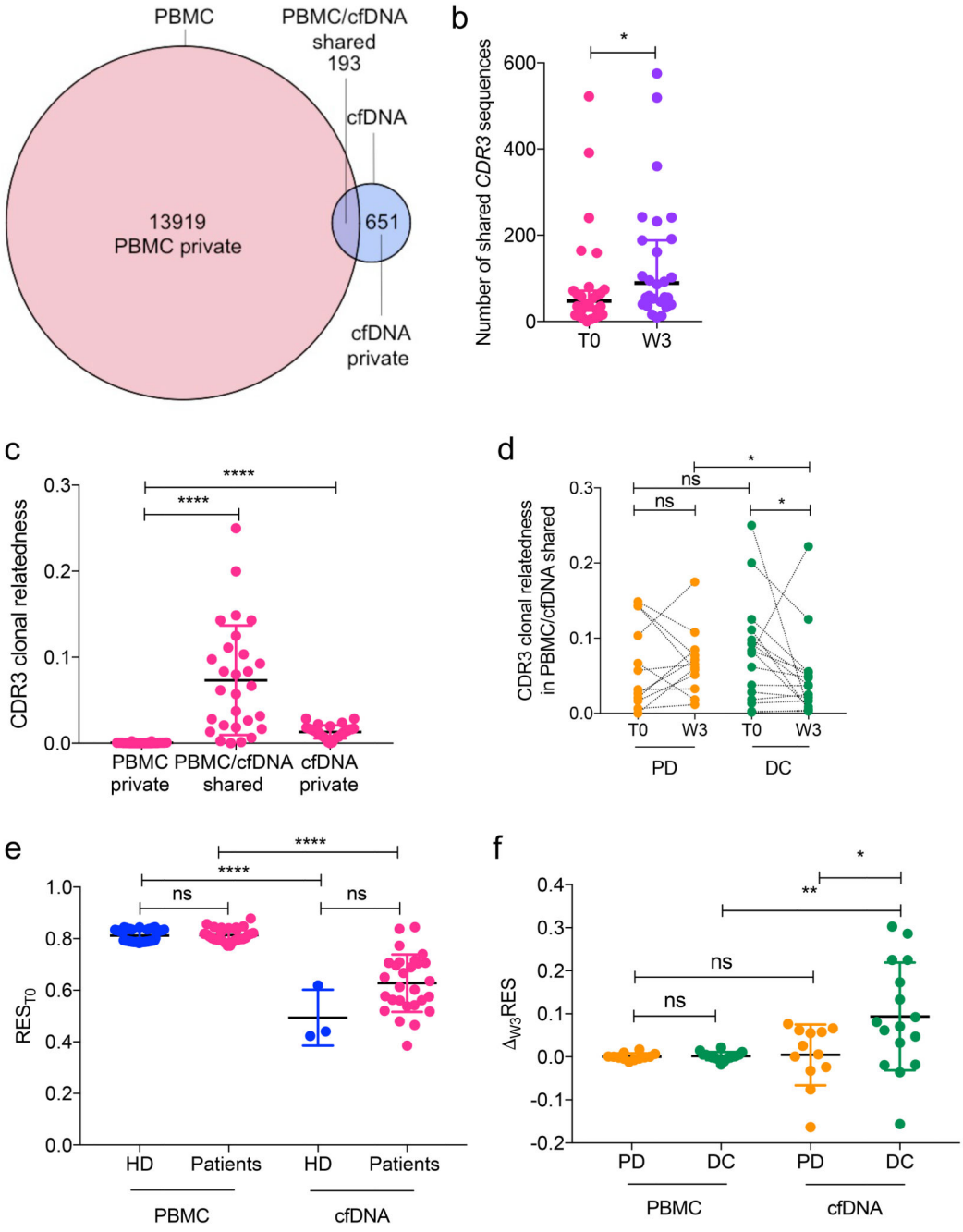

Figure 2. CPI induced peripheral T cell turnover.

a Venn diagram showing unique predicted productive *CDR3* sequences in PBMC (left, pink), PBMC/cfDNA-shared pool (intersection, purple) and cfDNA (right, blue) for patient #27 at T0 (Supplementary Table 2). **b** Total number of *CDR3* clones at T0 (pink) and W3 (purple) in the PBMC/cfDNA-shared pool (P=0.010, two-sided Wilcoxon test). **c** Clonal relatedness (maximum edit distance=3 amino acids) for CDR3 in the PBMC-private pool, PBMC/cfDNA-shared pool and cfDNA-private pools at T0. Horizontal lines: comparison of clonal relatedness between PBMC-private and cfDNA-private TCR sequences T0

(P<0.0001; two-sided Wilcoxon test; median was $0.3x10^{-3}$ and 0.01, respectively); comparison of clonal relatedness between PBMC-private and PBMC/cfDNA shared TCR sequences T0 (P<0.0001, two-sided Wilcoxon test; median was $0.3x10^{-3}$ and 0.06). **d** Clonal relatedness of CDR3 sequence in PBMC/cfDNA-shared pool at T0 and W3 for patients with progressive disease (the number of patients is 12, PD, orange) or disease control (the number of patients was 16, DC, green) at week 12. Comparison (horizontal lines) of clonal relatedness between: T0 PBMC/cfDNA-shared pool *TCR* sequences for patients with PD or DC (P=0.623, two-sided Mann-Whitney U test; median is 0.04 and 0.08); W3 PBMC/cfDNA-shared pool *TCR* sequences for patients with PD or DC (P=0.026; two-sided Mann-Whitney U test; median=0.06 and 0.03); T0 and W3 for the PBMC/cfDNA-shared pool *TCR* sequences for patients with PD (P=0.733; the number of patients was 12, two-sided Wilcoxon test; median=0.04 and 0.06) or DC (P=0.039; n=16, Wilcoxon test; median=0.08 and 0.03). **e** Pre-treatment *TCR* rearrangement efficiency score (RES_{T0}) of rearranged *CDR3* in healthy donors (HD) and patients on CPI in PBMC (P=0.445; median 0.83 and 0.81; the number of HD was 77 batches and the number of patients was 29; two-sided Mann-Whitney U test) and cfDNA (P=0.09, median 0.44 and 0.62; n=3 and 28; two-sided Mann-Whitney U test). Comparisons (horizontal lines) between: HD PBMC and cfDNA RES_{T0} (P<0.0001, two-sided Mann-Whitney U test); matched samples of patients' PBMC and cfDNA RES_{T0} (P<0.0001, Wilcoxon test). **f** Δ_{W3}RES (change in RES from T0 to W3) according to response group at week 12; **: P=0.008, two-sided Wilcoxon test, median was 0.001 and 0.08; *: P=0.037, two-sided Mann-Whitney U test, median=0.02 and 0.08. Total number of melanoma patients equal to 28; dot is one patient; error bar is standard deviation; connecting line is paired samples; horizontal line is median; T0 indicates pre-treatment; W3 indicates week 3; ns is not significant; * indicates P=0.05-0.01; **** indicates P<0.0001.

Europe PMC Funders Author Manuscripts

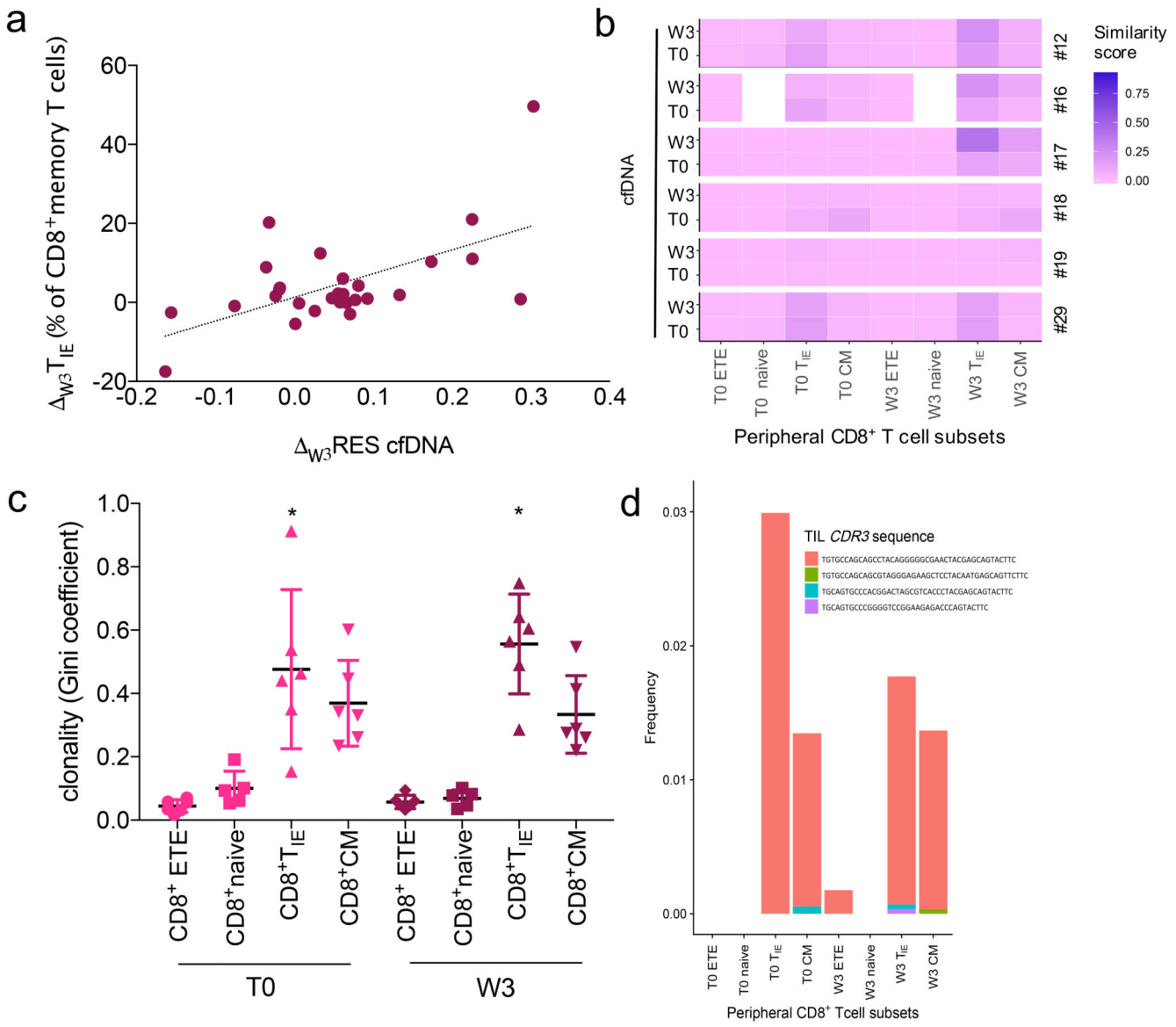

Figure 3. Identification of T_{IE} cells.

a Correlation between T_{IE} cell abundance ($\Delta_{W3}T_{IE}$) and changes in cfDNA RES (Δ_{W3}RES: RES_{W3}-RES_{T0},) at W3 relative to T0 (P=0.001; linear regression R^2=0.34, n=28 patients); dotted line is the linear regression line. **b** Similarity matrix of *TCR* sequences in cfDNA and peripheral CD8$^+$ T cell subsets. T_{CM}, T_{IE} T_{naive} and ETE similarity with cfDNA in 6 patients at T0 (median=0.026, 0.045, 0.004 and 0.003, respectively; P=0.0013; Friedman analysis of variance, Friedman statistics=15.64; patient #16 naive subset not assessed) and W3 (median=0.043, 0.136, 0 and 0.003, respectively; P<0.0001; Friedman analysis of variance, Friedman statistics=23.05; patient #16 naive subset not assessed). **c** Clonality (Gini coefficient) in peripheral CD8$^+$ T cell subsets. T_{IE} subset clonality relative to other subsets at baseline (T0, T_{IE} median clonality=0.46) and after the first cycle of CPI (W3, T_{IE} median clonality=0.61) in 6 matched patient samples (P=0.0006 and 0.0002, Friedman analysis of variance Friedman analysis of variance, Friedman statistics=12.6 and 13.08; patient #16

naive subset not assessed); error bar is standard deviation. The small sample size did not allow the comparison between responders (#16-18) and patients who progressed (#12,19,29); horizontal line is median; error bar is standard deviation. **d** Graph showing the frequency of pre-treatment TIL *CDR3* sequences in patient #12 sorted peripheral CD8+ T cell subsets at T0 and W3. Dot in **a** and **c** is a single patient.

Europe PMC Funders Author Manuscripts

Europe PMC Funders Author Manuscripts

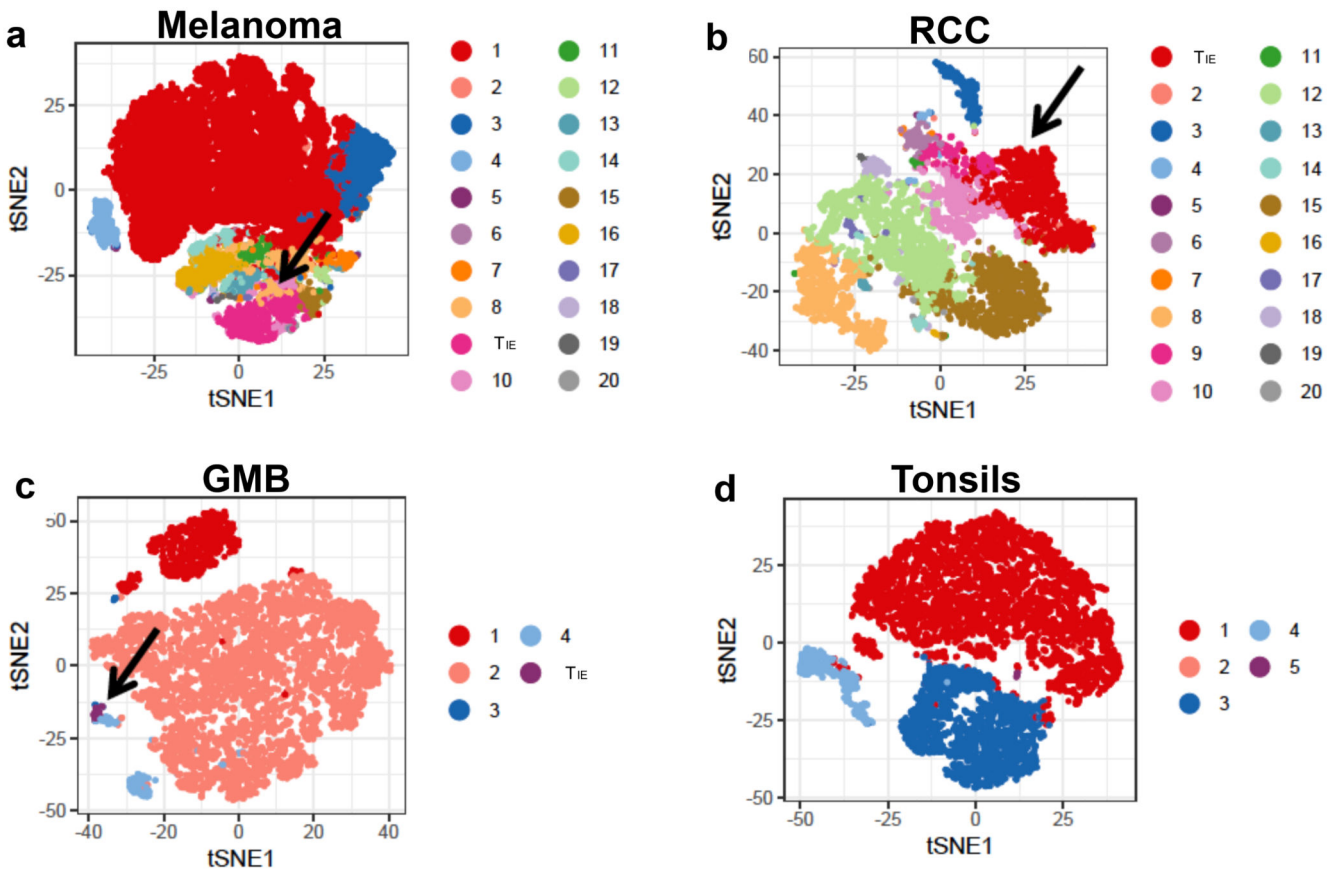

Figure 4. T_{IE} cells infiltrate tumors that respond to immunotherapy.

T-SNE (t distributed stochastic neighbor embedding) plots of biopsy cell clusters according to T cell surface markers in (**a**) melanoma (n=18 patient samples), (**b**) renal cell carcinoma (RCC, n=3 patient samples), (**c**) glioblastoma (GMB, n=3 patient samples), and (**d**) non cancerous tonsils (n=4 patient samples). Samples for this analysis were from reference #24. Black arrows highlight the clusters with the T_{IE} phenotype.

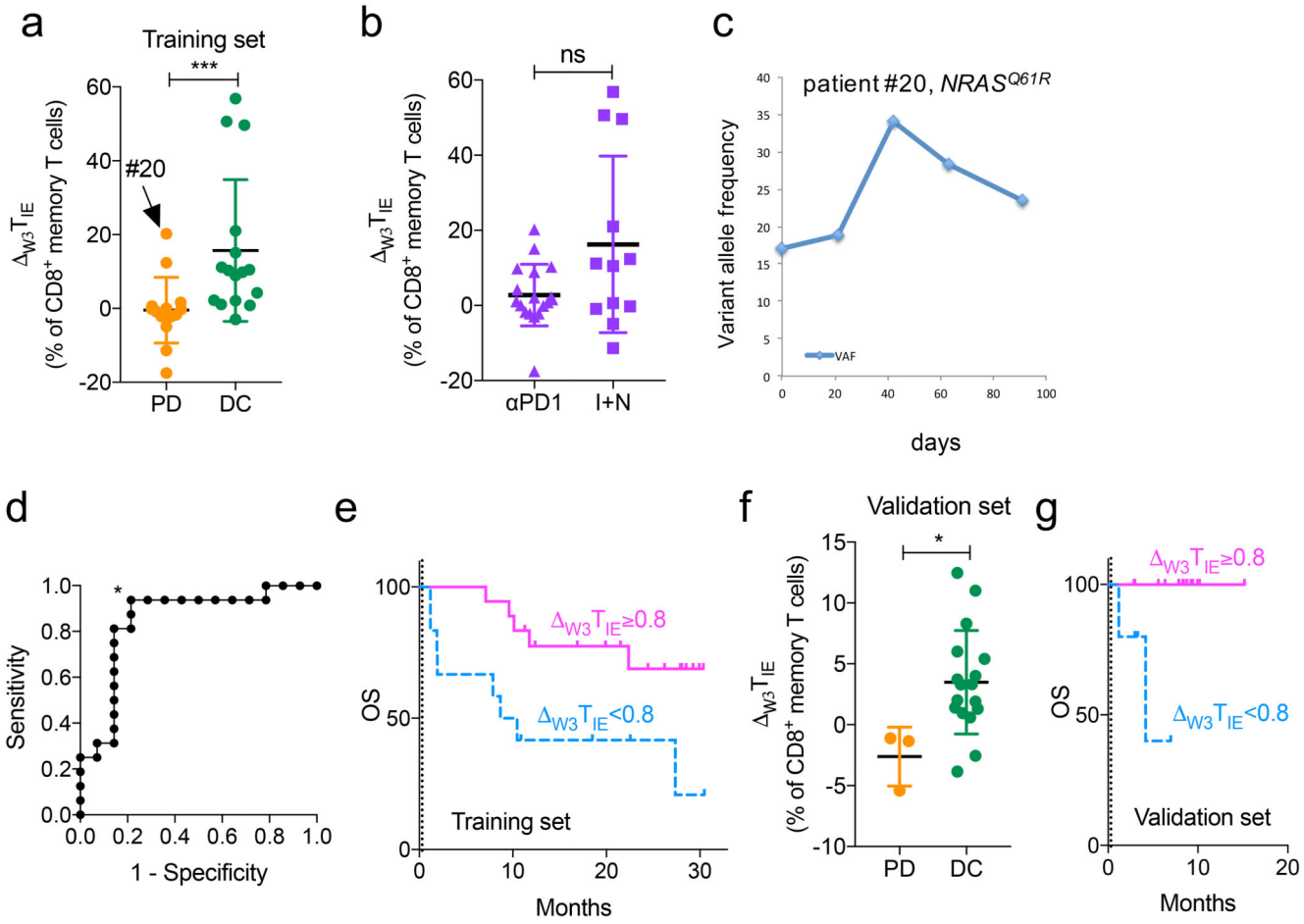

Figure 5. Peripheral T_{IE} cell expansion in response to first-line CPI.

a $\Delta_{W3}T_{IE}$ in patients with best response PD (orange, n=14, median=-0.58%) or best response DC (green, n=16, median=10.04%; ***: P=0.0007, two-sided Mann-Whitney U test) in the training set. Arrow: patient #20. **b** $\Delta_{W3}T_{IE}$ in patients receiving anti-PD1 monotherapy (αPD1, n=18, median=1.35%) or combination of ipilimumab plus nivolumab (I+N, n=12, median=10.84%; P=0.2, two-sided Mann-Whitney U test). **c** Variations over time (days from treatment initiation) of variant allele frequency (VAF) of mutant *NRAS*^{Q61R} measured in circulating tumor DNA by droplet digital PCR over the course of CPI treatment for patient #20 (arrow in **a**). Blood collection ceased after day 90 due to patient complications leading to patient death. **d** Receiver operating curve showing the sensitivity and false positive rate (1-specificity) of $\Delta_{W3}T_{IE}$ values in identifying the patients that will achieve disease control; *: maximum accuracy (cut-off=+0.8%). **e** Kaplan-Meier survival curves for patients with T_{IE} expansion ≥0.8% (pink, n=12; median survival not reached) at W3 compared to patients without T_{IE} expansion <0.8% (blue, n=18; median survival=9.6 months; P=0.013; log rank test), in the training set. **f** $\Delta_{W3}T_{IE}$ in patients with best response PD (orange, n=3, median=-1.3%) or best response DC (green, n=17, median=3.3%; *: P=0.019, two-sided Mann-Whitney U test) in the validation set. **g** Kaplan-Meier survival curves for patients with T_{IE} expansion≥0.8% (pink, n=15; median survival not reached) at W3 compared to patients without T_{IE} expansion≥0.8% (blue, n=5; median survival=4.2

months; two-sided log rank test, P=0.003), in the validation set. OS is overall survival; dot represents one patient; n represents patients; horizontal line is median; error bar is standard deviation; dotted vertical line is landmark at week 3.

Europe PMC Funders Author Manuscripts

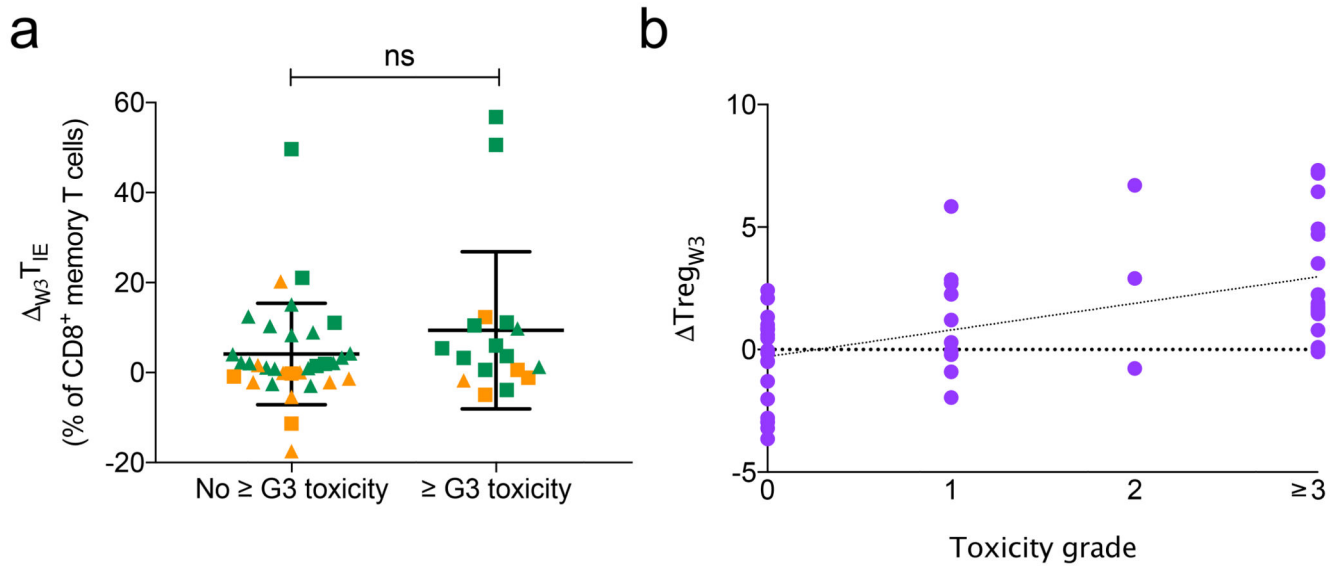

Figure 6. Expansion of a peripheral regulatory T cell subset associated with toxicity.

a Graph showing expansion of T_{IE} at W3 ($\Delta_{W3}T_{IE}$) in patients with no ≥grade 3 toxicity (median=1.6; n=33) or ≥grade 3 toxicity (median=3.72; P=0.347; n=17; two-sided Mann-Whitney U test). Line, median; error bar, standard deviation. Orange=PD, green=DC, dot=single patient, triangles=single agent anti-PD1, squares=combination ipilimumab +nivolumab. **b** Expansion of $CD3^+/CD4^+/CD8^-/CD25^+/CD127^{-/low}$ T_{reg} cells (Extended Data Figure 2g) at W3 ($\Delta_{W3}T_{reg}$) according to toxicity at any time between 2 weeks and 6 months (P<0.0001; n=50, two-sided linear regression analysis, R^2=0.29). Horizontal line is the median; error bar is standard deviation; orange represents PD; green represents DC; triangle represents one patient treated with single agent anti-PD1 drug; square represents one patient treated with combination ipilimumab+nivolumab; n represents patients; dotted line is linear regression line; ns is not significant; T0 is pre-treatment; W3 is week 3.

Europe PMC Funders Author Manuscripts

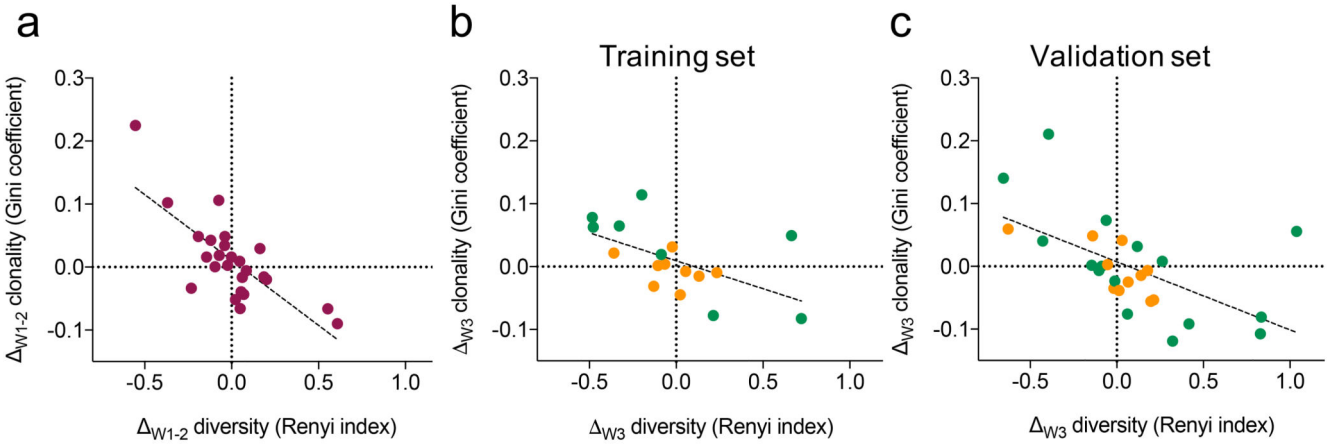

Figure 7. TCR repertoire evolution after immune-stimulation.

a Changes in *CDR3* clonality (Δclonality, Gini coefficient) and diversity (Δdiversity, Renyi index, alpha=1) in peripheral T cells from T0 to W1-2 in healthy donors who received anti-viral vaccination (n=25 healthy donor samples). **b** Changes in *CDR3* clonality (Δclonality, Gini coefficient) and diversity (Δdiversity, Renyi index, alpha=1) in peripheral T cells from T0 to W3 in the training cohort (The Christie NHS Foundation Trust) of advanced melanoma patients receiving first line anti-PD1 based immunotherapy (n=17 patients) who progressed (n=9 patients) or responded (n=8 patients) at week 12. **c** Δclonality (Gini coefficient) and Δdiversity (Renyi index, alpha=1) in peripheral T cells from T0 to W3 in the validation cohort (The Christie NHS Foundation Trust, Huang *et al.*[2] and Amaria *et al.*[26]cohort n=12 patients, n=4 patients and n=11 patients, respectively) of advanced melanoma patients who progressed (n=11 patients) or responded (n=16 patients) at week 12 of anti-PD1 based treatment. Dot is one healthy donor or patient; maroon represents healthy donors in the vaccination cohort; orange represents patients who progressed after 12 weeks of immunotherapy; green represents patients who achieved disease control after 12 weeks of immunotherapy; dotted line is the linear regression line.

Europe PMC Funders Author Manuscripts

Table 1

Tumor infiltrating T lymphocyte (TIL) CDR3 sequences also present in peripheral PBMC and cfDNA for patient #12 at T0 and W3.

The table shows the DNA (*$CDR3_{DNA1.1\text{-}4}$*) and their paired predicted protein ($CDR3_{prot1\text{-}4}$) sequences for the TCR that were identified in the pre-treatment tumor biopsy and also in the periphery, either in the T0 or W3 PBMC, or in the W3 cfDNA. For the proteins, the different CDR3 are color-coded, with $CDR3_{prot1}$ red, $CDR3_{prot2}$ purple, $CDR3_{prot3}$ green and $CDR3_{prot4}$ blue; the black text is the flanking TCR protein sequence. The red underlined bases in *$CDR3_{DNA1.2}$* highlights that *$CDR3_{DNA1.1}$* and *$CDR3_{DNA1.2}$* encode the same protein. Similarly, the red underlined base in *$CDR3_{DNA2.1}$* highlight that *$CDR3_{DNA2.1}$* and *$CDR3_{DNA2.2}$* encode the same protein. *CDR3 sequence count in the biopsy; #CDR3 sequence frequency in the sample.

Peripheral sample	Sequence		Count*	Frequency#	V gene name	D gene name	J gene name
T0 PBMC	$CDR3_{prot1}$	L E S P S P N Q T S L Y F C A S S L Q G A N Y E Q Y F G P G T R L					
	$CDR3_{DNA1.1}$	CTGGAGTCGCCCAGCCCCAACCAGACCTCTCTGTACTTCTGTGCCAGCAGCCTACAGGGGGCGAACTACGAGCAGTACTTCGGGCCGGGCACCAGGCTC	7	0.000599	TCRBV27-01	TCRBD01-01	TCRBJ02-07
	$CDR3_{DNA1.2}$	CTGGAGTCGCCCAGCCCCAACCAGACCTCTCTGTACTTCTGTGCCAGCAGCCTACAGGGGGCGAACTACGAGCAGTACTTCGGGCCAGGCACGCGGCTC	1	8.56E-05	TCRBV27-01	TCRBD01-01	TCRBJ02-05
	$CDR3_{prot2}$	L T V T S A H P E D S S F Y I C S A R G P E E T Q Y F G P G T R L					
	$CDR3_{DNA2.1}$	CTGACAGTGACCAGTGCCCATCCTGAAGACAGCAGCTTCTACATCTGCAGTGCCCGGGGTCCGGAAGAGACCCAGTACTTCGGGCCAGGCACGCGGCTC	1	8.56E-05	TCRBV20	TCRBD02-01	TCRBJ02-05
	$CDR3_{prot3}$	S D L E L G D S A L Y F C A S S V G R S S Y N E Q F F G P G T R L					
	$CDR3_{DNA3}$	AGCTCTCTGGAGCTGGGGGACTCAGCTTTGTATTTCTGTGCCAGCAGCGTAGGGAGAAGCTCCTACAATGAGCAGTTCTTCGGGCCAGGGACACGGCTC	1	8.56E-05	TCRBV09-01	TCRBD02-01	TCRBJ02-01
W3 cfDNA	$CDR3_{prot4}$	S A H P E D S S F Y I C S A R D W L A G D T G E L F F G E G S R L					
	$CDR3_{DNA4}$	AGTGCCCATCCTGAAGACAGCAGCTTCTACATCTGCAGTGCTAGAGATTGGCTAGCGGGAGACACCGGGGAGCTGTTTTTTGGAGAAGGCTCTAGGCTG	2	0.0069444	TCRBV20	TCRBD02-01	TCRBJ02-02
W3 PBMC	$CDR3_{prot1}$	L E S P S P N Q T S L Y F C A S S L Q G A N Y E Q Y F G P G T R L					
	$CDR3_{DNA1.1}$	CTGGAGTCGCCCAGCCCCAACCAGACCTCTCTGTACTTCTGTGCCAGCAGCCTACAGGGGGCGAACTACGAGCAGTACTTCGGGCCGGGCACCAGGCTC	10	0.0016176	TCRBV27-01	TCRBD01-01	TCRBJ02-07
	$CDR3_{prot2}$	L T E T S A H P E D S S F Y I C S A R G P E E T Q Y F G P G T R L					
	$CDR3_{DNA2.1}$	CTGACAGTGACCAGTGCCCATCCTGAAGACAGCAGCTTCTACATCTGCAGTGCCCGGGGTCCGGAAGAGACCCAGTACTTCGGGCCAGGCACGCGGCTC	1	0.000162		TCRBD02-01	TCRBJ02-05
	$CDR3_{DNA2.2}$	CTGACAGTGACCAGTGCCCATCCTGAAGACAGCAGCTTCTACATCTGCAGTGCCCGGGGTCCGGAAGAGACTCAGTACTTCGGGCCAGGCACGCGGCTC	1	0.000162	TCRBV20	TCRBD02-01	TCRBJ02-05